metals

MDPI

Article

Effect of Lower Sheet Hole on Joint Strength in Pre-Holed Hot Clinching of Al-Si-Coated 22MnB5 Steel Sheets

Jarupong Charoensuk [1], Takuma Iwai [2], Taiga Hongo [2], Tomoyoshi Maeno [2,*] and Surasak Suranuntchai [1,3,*]

[1] Department of Tool and Materials Engineering, King Mongkut's University of Technology Thonburi, 126 Pracha Uthit Rd., Bang Mod, Thung Khru, Bangkok 10140, Thailand; jarupong.charo@mail.kmutt.ac.th
[2] Division of Systems Research, Faculty of Engineering, Yokohama National University, Yokohama 240-8501, Kanagawa, Japan
[3] Faculty of Engineering, Kasem Bundit University, Rom Klao Campus, 60 Rom Klao Rd., Min Buri, Bangkok 10510, Thailand
* Correspondence: maeno-tomoyoshi-yf@ynu.ac.jp (T.M.); surasak.sur@kmutt.ac.th (S.S.)

Abstract

This study introduced a pre-holed hot clinching process for hot stamping patchwork blanks, using the lower sheet pre-hole as a forming cavity to facilitate material flow and minimize deformation resistance. Evaluated through mechanical testing and finite element analysis (FEA), the process induced ausforming and maintained material homogeneity (~500 HV), and an optimal interfacial gap up to 10 mm effectively prevented localized soft-zone fractures. Results identified interfacial slip, driven by a critical differential surface expansion rate, as the primary mechanism for geometric anchoring and solid-state bonding. Experimental validation established optimal joining at a 60% penetration ratio and a 0.9 hole-to-punch diameter ratio. While prior studies on forge joining reported average maximum strengths limited to 1.2 kN due to the absence of a mechanical hook, the optimized pre-holed joints in this work achieved a superior tensile shear capacity of 11.5 kN. Furthermore, the cross-tension load reached 0.77 kN, representing a nearly tenfold increase compared to the 0.08 kN observed in the no-hole with offset condition. These results demonstrate that the pre-holed hot clinching method significantly enhances joint integrity while reducing the forming load from 70 kN without a pre-hole to 12 kN with a 10 mm pre-hole.

Keywords: hot stamping; patchwork blanks; tailored blank; finite element analysis; press hardening; pre-holed hot clinching; solid-state joining; ausforming

Check for updates

Academic Editor: Zhengwei Li

Received: 3 April 2026
Revised: 6 May 2026
Accepted: 9 May 2026
Published: 12 May 2026

Copyright: © 2026 by the authors. Licensee MDPI, Basel, Switzerland. This article is an open access article distributed under the terms and conditions of the Creative Commons Attribution (CC BY) license.

1. Introduction

The automotive parts industry has been heavily focused on improving the strength of components, leading to substantial advancements in materials and manufacturing processes. These improvements are driven by the goals of reducing vehicle weight, enhancing driver safety, conserving energy, and lowering carbon dioxide emissions, among others [1–3].

Hot stamping has been widely used to reduce automobile weight and improve collision safety, particularly for producing ultra-high-strength steel components that enhance crashworthiness [4–6]. The process involves shaping steel sheets at temperatures above their recrystallization temperature. The subsequent quenching transforms the steel from austenite into martensite, yielding enhanced mechanical properties and a tensile strength of 1500 MPa and minimal elastic recovery (springback) [7]. Additionally, the capability

of forming parts in a single operation enables the use of thinner materials, which in turn reduces part weight and material costs.

The enhancement of vehicle crashworthiness and the simultaneous reduction of structural mass are frequently achieved through optimization strategies involving variable material thickness. Part thickness is tailored to local mechanical needs by using more material in high-stress areas and less in lower-load regions, thereby allowing manufacturers to optimize weight distribution without compromising structural integrity. Known as tailored blank technology [8–10]. The implementation of high-strength tailor-welded blanks has demonstrated significant potential for vehicle lightweighting; however, the adoption of these processes is often constrained by their inherent manufacturing complexity and the necessity for substantial capital investment.

Broadly, tailored blanks are defined by localized variations in either gauge thickness or material properties and are categorized into several distinct methodologies [11]:

- Tailor Welded Blanks (TWBs): Fabricated by joining discrete sheets of differing grades or thicknesses into a single continuous sheet, typically via laser or mash seam welding.
- Tailor Rolled Blanks (TRBs): Produced through a flexible rolling process that achieves a continuous, profiled thickness distribution within a single metallic sheet.
- Tailor Heat-Treated Blanks: Characterized by localized microstructural modifications induced through targeted thermal cycles to alter regional mechanical performance.
- Patchwork Blanks: Comprised of a primary substrate locally reinforced by secondary high-strength material overlays to provide targeted structural support.

Hot stamping of patchwork blanks represents an effective alternative for structural optimization [12,13]. Unlike tailor-welded blanks, which are joined edge-to-edge, this technology utilizes overlapping patches spot-welded onto a base material to provide highly localized reinforcement. This approach offers superior flexibility, allowing for targeted strength increases in complex internal zones without requiring modifications to the primary sheet. While combining hot stamping with patchwork blanks is expected to produce lighter and stronger car bodies, the process introduces significant manufacturing challenges that can adversely affect the formability of the reinforced areas.

Although resistance spot welding (RSW) remains the conventional choice for joining ultra-high-strength steel patchwork blanks in hot stamping [13,14], this joining method introduces significant manufacturing constraints. The high density of weld points can induce localized structural rigidity, which frequently compromises material formability and results in defects such as wrinkling or fracturing during the stamping process [15,16]. Furthermore, the uneven thickness of the blank causes non-uniform different rates. This inconsistent temperature distribution between the base sheet and the reinforced zones impedes uniform plastic flow and may facilitate the degradation of protective Al-Si coatings prior to final forming [16].

Recent studies have increasingly relied on computational modeling to investigate these complex thermo-mechanical behaviors and mitigate forming defects. However, the inherent complexity of these models significantly increases computational time and developmental costs. Specifically, Zhang et al. [15] developed a high-temperature spot welding failure model and a thermal–mechanical FEM to predict welding failures and thickness distribution in hot-stamped A-pillar patchworks. Lei et al. [12] studied hot stamping of patchwork blanks, developed and validated an FE model to predict welding failures, and optimized process parameters for improved component quality.

Alternative joining strategies offer a more direct solution to these manufacturing and computational burdens. Mori et al. [17] introduced the pivotal concept of using plastic deformation as a primary joining mechanism. This approach is fundamentally divided into two categories: mechanical joining, which relies on physical interlocking, and

metallurgical joining, which establishes a bond within the material structure. By utilizing these deformation-based techniques, manufacturers can effectively avoid the common defects associated with resistance spot welding in patchwork blanks.

In the context of mechanical joining, specifically the process of mechanical clinching, a punch and die assembly is utilized to establish a mechanical interlock between two metal sheets [18,19]. Although this technique is highly effective in automotive manufacturing, offering secure connections without the need for auxiliary fasteners, the conventional cold clinching of ultra-high strength steel is inherently challenging [20]. The material's notoriously low ductility frequently leads to severe material fractures within the joint zone during cold forming. Researchers have explored various modifications to circumvent this limitation; for instance, Abe et al. [21] used a clinch-bonding process with a fine-particle adhesive, optimizing the parameters to successfully join 980 MPa steel to aluminum without defects. Furthermore, Lee et al. [22] introduced hole clinching to overcome ductility constraints in dissimilar material joining. However, cold hole-clinching often generates excessive forming loads that lead to premature punch fracturing. Therefore, the forming load must be minimized through thermal assistance to ensure process feasibility and tool longevity.

Ultimately, to comprehensively address these structural defects and fundamentally enhance joint integrity, recent advancements have incorporated hot stamping technology into the clinching sequence, utilizing elevated temperatures to overcome the cold-forming limitations of ultra-high-strength steel. As demonstrated by Chen et al. [23], performing clinching at elevated temperatures facilitates superior material flow, enabling a secure interlock in components otherwise prone to failure. However, the reliance on specialized die cavities and blank holders significantly increases tooling complexity and manufacturing costs. More importantly, the intricate cavity geometry often leads to non-uniform thermal distribution and inconsistent quenching rates. This sensitivity makes controlling final mechanical properties, such as preventing soft spots or excessive brittleness, exceptionally difficult, thereby necessitating an optimization of process parameters.

Beyond mechanical interlocking, metallurgical joining, encompassing techniques like cold pressure welding, provides an alternative approach driven by severe plastic deformation [24]. In these solid-state welding processes, intense compressive forces fracture surface oxide layers and disperse interfacial contaminants. The newly exposed, nascent metal surfaces are then forced into intimate contact, while the localized heat generated from internal friction and plastic work softens the material to accelerate the metallurgical bond. Building upon this paradigm, Yamagishi et al. [25,26] developed cold spot forge-welding (CSFW) for high-efficiency solid-state joining. Demonstrating the process's versatility, their research encompassed both the multilayer bonding of A1N30H/A1050 foils for electrode structures and the fabrication of dissimilar Cu/Al joints, where the effects of bonding temperature and reduction ratio were evaluated. The fundamental advantage of CSFW is its application of instantaneous, high-intensity pressure at low temperatures, which meticulously regulates interfacial reactions and inhibits the formation of brittle intermetallic compounds (IMCs) that frequently compromise traditional fusion welds.

Adapting this solid-state bonding mechanism to high-temperature environments, Charoensuk et al. [27] proposed a novel forge joining technique that integrates the hot stamping process and solid-state joining into a single operation. By utilizing the aforementioned plastic flow principles during the hot stamping phase, this method establishes a direct metallurgical connection without the need for auxiliary fasteners or filler materials, representing a highly efficient manufacturing solution. Despite these advantages, the process currently exhibits critical limitations that require further investigation. Foremost, the mechanical strength of the resulting joints remains inferior to that of conventional resistance spot welding. A promising strategy to enhance this load-bearing capacity in-

volves leveraging the inherent mechanical strength of the patch material itself to act as a structural reinforcement. Furthermore, the complex thermo-mechanical dynamics, specifically the function of the pre-hole as an internal forming cavity during high-temperature stamping, have yet to be thoroughly explored. Consequently, a significant research gap remains in systematically optimizing the critical process variables for this specialized joining technique.

This research investigates pre-holed hot clinching, an innovative methodology integrating the hot stamping process and mechanical joining for Al-Si-coated 22MnB5 steel. The study specifically examines the concept of utilizing the pre-hole in the lower sheet as a functional forming cavity to facilitate a mechanical joint. The primary aim is to optimize joint strength and minimize joining loads compared to conventional forge joining. Furthermore, the investigation evaluates the influence of hole diameter and penetration ratio on structural integrity, alongside the effects of quenching on microstructure and hardness. Through combined experimental analysis and numerical simulations, this work validates the industrial feasibility of the methodology and clarifies the fundamental mechanics of using internal cavities for high-strength steel joining.

2. Materials and Methods

2.1. Pre-Holed Hot Clinching Method of Patchwork Blanks in a Hot Stamping Process

Resistance spot welding before hot stamping is conventional method for ultra-high strength steel patchwork. However, the reduced formability of the welded zones makes them prone to rupture, while stress concentration and restricted material flow increase the risk of wrinkling and cracking during forming [15,16]. To overcome these limitations of conventional methods, forge joining was implemented within a single hot stamping operation, as shown in Figure 1. In this process, bonding occurs rapidly between nascent surfaces as plastic deformation removes surface contaminants, such as oxides. However, the joint strength of the forge-joined interfaces is fundamentally limited because it relies solely on interfacial metallic bonding, without any mechanical hooking or physical engagement between the sheets. This lack of mechanical reinforcement makes the joint highly prone to brittle fracture under deformation, meaning the tensile strength of 1.5 GPa achieved through the hot stamping process remains entirely unutilized. Consequently, this results in an average joint strength of approximately 1.2 kN, a value significantly lower than the 7.91 kN minimum required for Class B spot welding of 1.6 mm steel sheets under the Japanese Industrial Standard (JIS Z 3140) [28]. As there is currently no specific international standard for hot-stamped 22MnB5 steel, the standard values for general structural steel 270–370 $N \cdot mm^{-2}$ were adopted. These values represent the absolute maximum tensile shear strength specified within existing standards, serving as a baseline for evaluating the performance of the developed joints. To bridge this gap and meet industrial requirements, pre-holed hot clinching was investigated as a complementary mechanical joining method to introduce physical engagement and enhance joint strength, as shown in Figure 2.

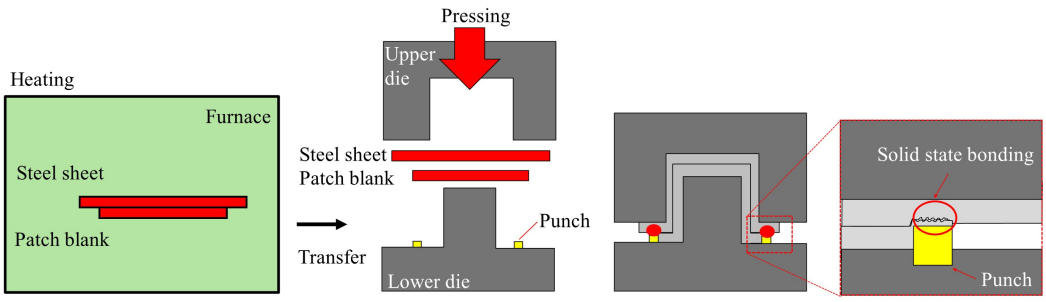


Figure 1. Forge joining in hot stamping process of patchwork blanks.

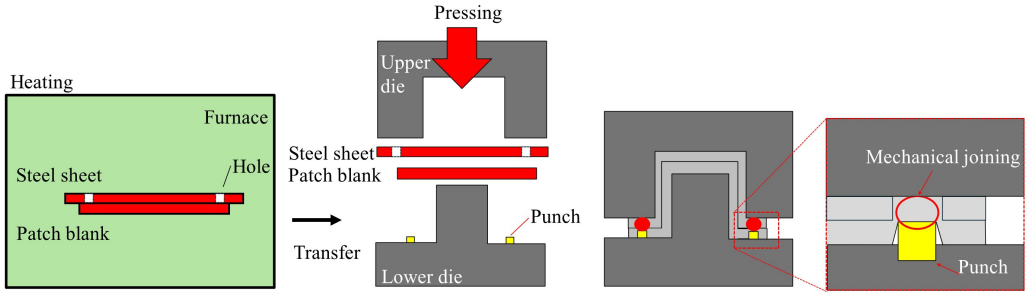


Figure 2. Pre-holed hot clinching in hot stamping process of patchwork blanks.

Joining was conducted exclusively using a flat die. A schematic of the experiment setup and the test specimen is presented in Figure 3. Both the upper and lower sheets are made of 22MnB5 ultra-high strength steel, with the lower sheet being pre-holed prior to joining. The nominal thickness of the steel sheets was 1.6 mm, and the specimen width was 20 mm. The experiment utilized a circular punch, and the chemical compositions and mechanical properties are detailed in Tables 1 and 2, respectively.

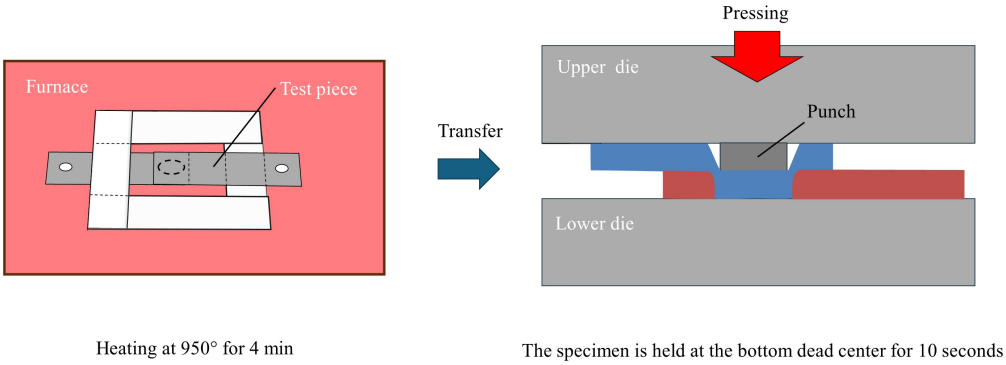


Figure 3. Experimental setup for pre-holed hot clinching of strip sheets utilizing flat tools.

Table 1. Chemical composition of 22MnB5 steel sheet.

Element	C	Si	Mn	P	B
Composition (mass%)	0.21	0.25	1.2	0.015	0.0014

Table 2. Mechanical properties of die-quenched 22MnB5 steel sheet.

Tensile Strength	Thickness	Total Elongation	Vickers Hardness
1.53 GPa	1.6 mm	6.8%	480 HV1

Conventional clinching relies on a contoured die to shape the materials into an interlocking connection, with the die's geometry determined by specific parameters. The tool design, customized to factors such as material thickness and strength, ensures proper joint formation. The substitution of a complex-shaped die with a flat die simplifies the manufacturing process by eliminating the need for specialized die geometry. Consequently, this fundamental change in the clinching method leads to a substantial reduction in tooling and production costs.

The process utilized 22MnB5 steel sheets, which initially exhibited ferritic and pearlitic microstructures at room temperature. These sheets were joined and quenched using a flat die. To ensure full austenitization and enhance ductility, the specimens were heated in an electric furnace at 950 °C for 4 min, resulting in the formation of an austenitic structure. Subsequently, the specimens were transferred within 5 s, and the joining operation was conducted with the hole center coaxially aligned with the punch center. During joining, a

10 s hold at the bottom dead center was maintained, serving as the quenching phase. The die quench process, with a cooling rate exceeding 30 °C/s [4], ensures a transformation from austenite to martensite, leading to a corresponding increase in strength.

The pre-holed hot clinching process involves pressing the upper sheet downward with a punch into the cavity of the lower sheet, as illustrated in Figure 4. This mechanical action induces material deformation, causing the upper sheet to flow and expand radially into the lower sheet's pre-hole to establish a secure joint. This approach fundamentally differs from conventional clinching, where the joint geometry is primarily governed by the die cavity's profile. In the pre-holed method, however, the joining mechanism is defined by the pre-existing hole geometry of the lower sheet. To ensure a proper joint precise alignment between the punch center and the hole center in the lower sheet is essential.

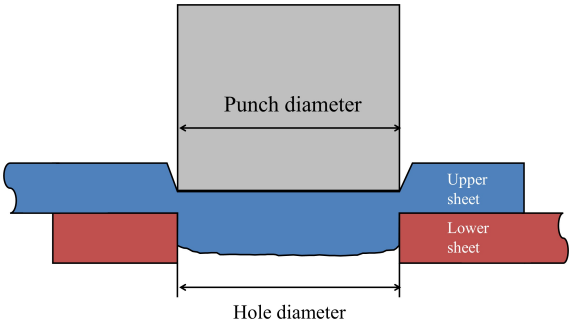


Figure 4. Schematic illustration of the joint cross-section in pre-holed hot clinching.

Joining was performed utilizing a press machine (Amada Machine Tools, Ltd., Isehara, Japan, electric servo press SDE-8018BO), with die dimensions provided in Ref. [27]. The die set conforms to the Japanese Industrial Standards (JIS) [29] and is constructed primarily from S50C carbon steel. The die and punch were fabricated from heat-treated SKS alloy tool steel and SKD11 cold work tool steel, respectively. To investigate joint characteristics, pre-holed hot clinching experiments were conducted on stainless steel shim tape, as schematically depicted in Figure 5. Before the experiments, the specimens were temporarily secured at the corners using low-current spot welding to ensure precise positioning during the transfer process. Due to the minimal heat input, any potential localized heat-affected zones (HAZ) were effectively eliminated during the subsequent austenitization stage [30], ensuring microstructural homogeneity throughout the specimens before the forming phase. The penetration ratio x (%), defined as the penetration depth of the punch at the bottom dead center relative to the total sheet thickness, is derived based on the geometric parameters shown in Figure 6 and Equation (1).

$$x = \frac{D}{t_0} \times 100 \quad (1)$$

where x is the nominal penetration ratio (%). D is the penetration depth of the upper die at the bottom dead center. t_0 is the initial total thickness of the steel sheets.

2.2. Joint Strength Evaluation Method

The mechanical strength of the joints was evaluated through tensile shear and cross-tension tests. Figure 7a illustrates the tensile shear test setup for the joined specimens. The cross-tension test is depicted through the illustration in Figure 7b, and the dimensions of the cross-tension specimens are shown in Figure 7c. Both tests were conducted at a constant stroke speed of 5 mm/min. The testing conditions were established and adapted in accordance with the Japanese Industrial Standard (JIS Z 3136 and JIS Z 3137) [31,32].

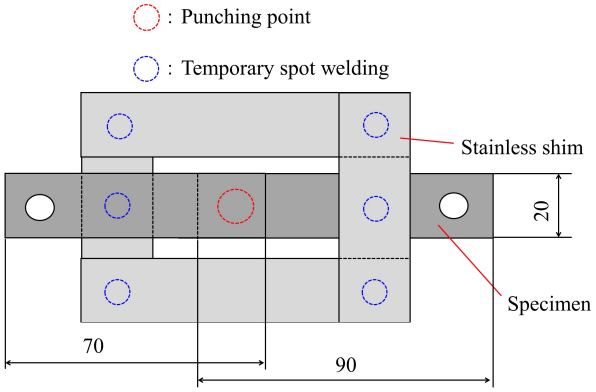


Figure 5. Dimensions of specimen and stainless shim for pre-holed hot clinching experiment [Unit: mm].

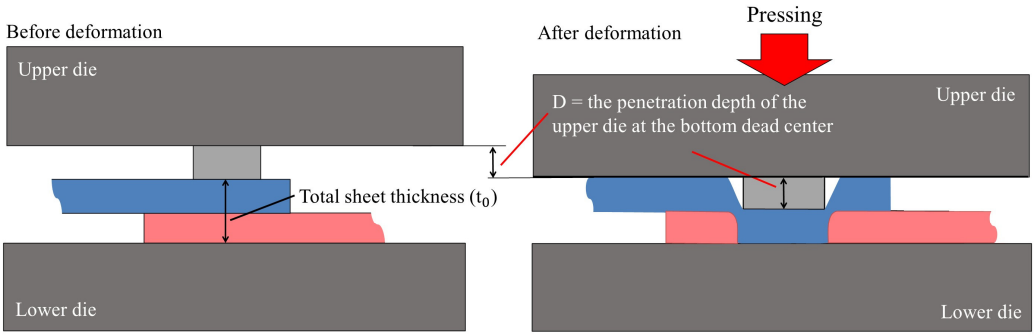


Figure 6. Schematic representation of the penetration depth and the derivation of the nominal penetration ratio x at the bottom dead center.

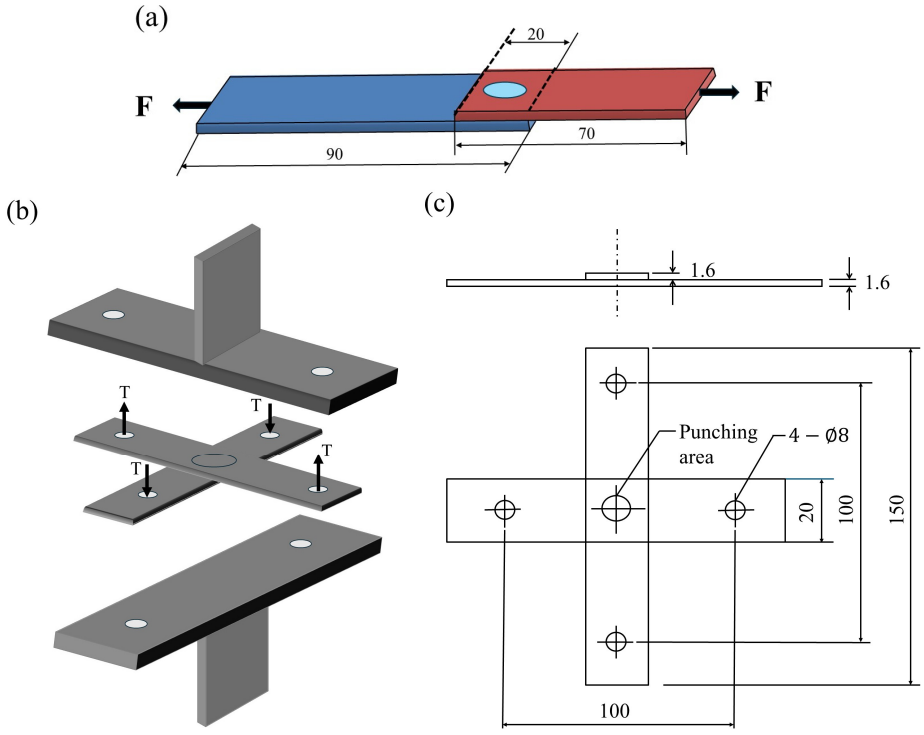


Figure 7. Experimental evaluation of joint strength: (**a**) tensile shear test; (**b**) cross tension test; and (**c**) cross tension specimen dimensions [unit: mm].

2.3. Simulation Analysis Method for Pre-Holed Hot Clinching

The pre-holed hot clinching procedure was simulated utilizing Simufact Forming 2025, which operates on the nonlinear MSC Marc solver. Adhering to the protocols established

in our prior study [27], the simulation was executed using a thermo-mechanical coupled analysis with a static implicit approach.

To accurately capture the characteristics of the 22MnB5 press-hardened steel, a comprehensive thermo-mechanical-metallurgical model was implemented. This framework relied on dynamic multi-dimensional linear interpolation alongside tabulated flow curve data from JMATPRO 2024, aligning with the Numisheet 2008 benchmark [33–35]. Standard material parameters from the Simufact database were selected to guarantee reliable and repeatable outcomes under varying conditions.

Consistent with previous methodologies, the specimens were defined as elastic-plastic to simulate both physical deformation and heat transfer, whereas the tooling was modeled strictly as rigid bodies for thermal exchange. Starting temperatures were established at 750 °C for the steel blanks and 20 °C for both the tools and the surrounding environment. During the process, the upper die and punch descended at a uniform rate of 25 mm/s. Continuous remeshing was enabled to preserve element integrity throughout the deformation phase, with both specimens utilizing the exact hexahedral mesh dimensions detailed in the previous study [27].

3. Results and Discussions

3.1. Effect of Pre-Hole Diameter of Lower Sheet on Joint Strength

A circular pre-hole was prepared in the lower sheet, and joining was performed by using a punch to facilitate the flow of the upper sheet material into the pre-hole. A circular punch with a diameter of 10 mm was employed. To identify the optimal conditions for achieving a stronger joint, the diameter of the pre-hole was varied at 0 mm, 5 mm, 7.5 mm, 9 mm, 10 mm, 11 mm, and 12.5 mm. To ensure sufficient material around the joint, the center of the pre-hole was positioned 10 mm from the edges in both the width and longitudinal directions of the sheet. The punch position was coaxially aligned with the center of the pre-hole. The separated surfaces of the actual specimens after the tensile shear tests are shown in Figure 8. For all pre-hole diameters, the upper sheet material sufficiently filled the hole. In the surrounding areas, separation of the coating layer was observed, accompanied by plastic deformation due to compression. The penetration ratio in sheet thickness was set at 40% for this experiment.

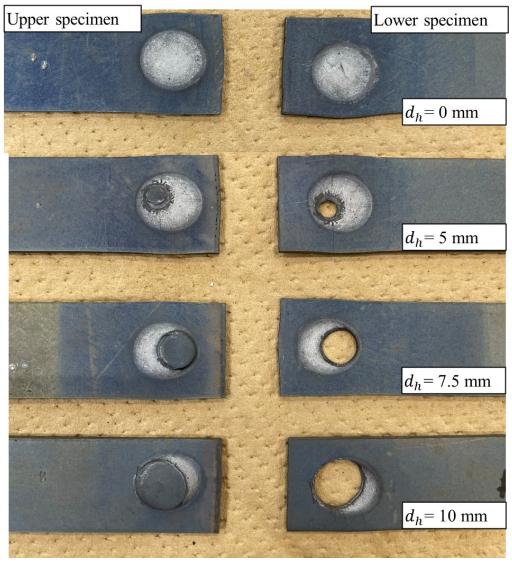


Figure 8. Interfacial surfaces of pre-holed hot clinched specimens after tensile shear testing.

Tests were conducted at least five times for each pre-hole diameter, and the resulting tensile shear loads are presented in Figure 9. In this context, the "no hole with offset" condition refers to a punch position being offset by 10 mm from the longitudinal edge. Conversely, the "no hole without offset" condition represents a position with no offset from the longitudinal edge. The specimen with no hole without offset is equivalent to forge joining, providing a baseline for comparison with the pre-holed hot clinching method. The results showed that the no hole without offset (forge joining) condition slightly outperformed the with-offset condition in terms of strength; however, such variations were minor and did not represent a significant difference in joint strength.

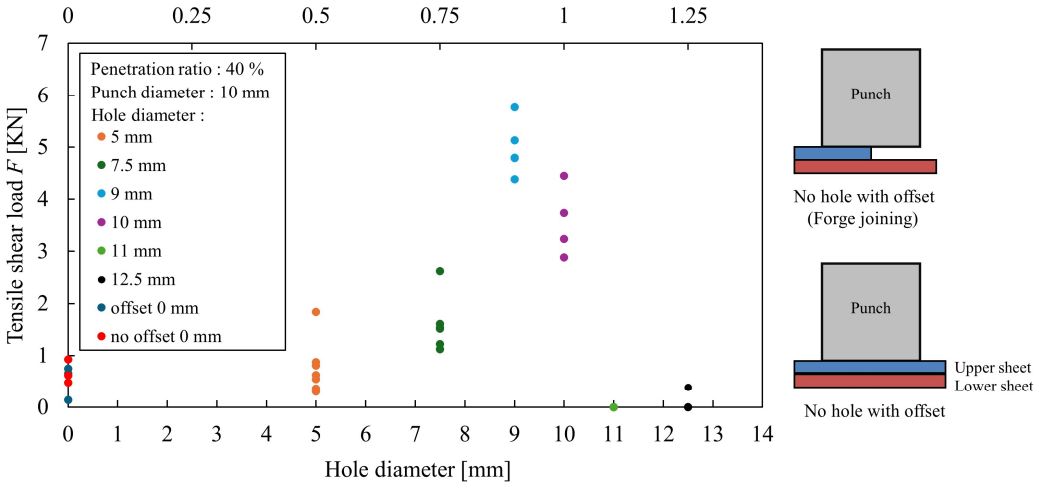


Figure 9. Relationship between pre-hole diameter and maximum tensile shear load.

The joint strength exhibited a clear upward trend as the pre-hole diameter increased. Initially, at a diameter of 5 mm, the tensile shear strength was comparable to that of forge joining under similar conditions, with average values of 0.67 kN for forge joining and 0.76 kN for the 5 mm pre-hole. However, as the diameter increased to 7.5 mm, the pre-holed hot clinching method demonstrated significantly higher strength than the forge joining, with an average value of 1.6 kN. The tensile shear strength peaked at a diameter of 9 mm, reaching a maximum value of 5.76 kN. This indicates that the strongest joint was achieved at a hole-to-punch diameter ratio of 0.9. This increase in strength is likely attributed to the increased circumference of the mechanical joint zone as the pre-hole diameter grows. Under tensile shear loading, the joint's load-bearing capacity heavily depends on the volume of the upper specimen extruded into the lower sheet hole. Specifically, a 7.5 mm pre-hole produces a significantly larger extruded button than a 5 mm hole. This effectively enlarges the shear-resisting cross-sectional area, enabling the joint to withstand higher loads before failure occurs. The tensile shear load reaches its peak at a pre-hole diameter of 9 mm before declining at 10 mm. At 9 mm, the upper specimen maintains sufficient neck thickness while forming a large extruded button, thereby maximizing the effective shear-resisting area. However, when the pre-hole increases to 10 mm, matching the punch diameter, the resulting zero clearance induces severe localized deformation. This causes excessive wall thinning (necking) of the upper specimen along the punch edge during the downward stroke. Consequently, this severely thinned region acts as a critical weak point, reducing the joint's load-bearing capacity. Conversely, the strength dropped dramatically at diameters of 11 mm and 12.5 mm, which occurred when the punch diameter was smaller than the pre-hole diameter, leading to a failure in effective joining. However, at a pre-hole diameter of 7.5 mm, some specimens failed to join. Photographs of these trials are shown in Figure 10. Due to a positioning error, the pre-hole was significantly misaligned with the punch compression area, resulting in only approximately 20% of the material flowing into

the pre-hole. This suggests that this method requires more precise alignment compared to the forge joining method.

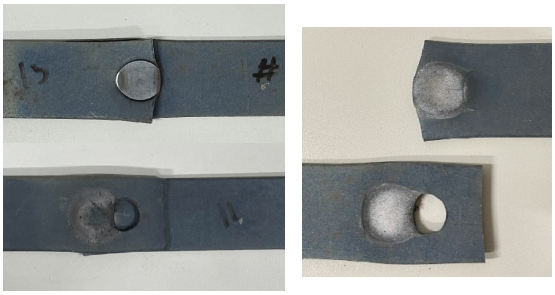


Figure 10. Misalignment joining of a specimen with a 7.5 mm pre-hole diameter.

In cases where the pre-hole diameter was 12.5 mm (exceeding the 10 mm punch diameter), the joint strength decreased significantly, or joining was not achieved at all. As shown in Figure 11, for pre-hole diameters of 7.5 mm and 10 mm, the upper specimen material sufficiently filled the lower specimen pre-hole (indicated by the red area). On the other hand, at a diameter of 12.5 mm, the volume of material displaced by the punch was less than the volume of the pre-hole cavity, resulting in incomplete filling (filling on one side only). This incomplete filling likely led to premature separation, causing the drastic reduction in joint strength. Future studies should utilize robotic arms to simultaneously address alignment issues and reduce transfer time. By preventing alignment errors and minimizing the temperature drop associated with prolonged delivery, this approach will effectively prevent process variation and joining failures.

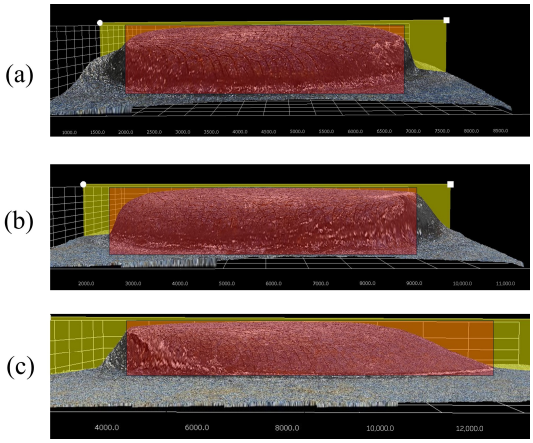


Figure 11. Appearance of the joint surface on the upper specimen (Red indicates lower specimen cavity): (**a**) 7.5 mm; (**b**) 10 mm; and (**c**) 12.5 mm.

Figure 12 illustrates the load-stroke curves obtained from the tensile shear tests for specimens joined with varying pre-hole diameters. All specimens exhibited a consistent trend characterized by a steady increase in load followed by sudden separation. Overall, the displacement (stroke) at separation tended to increase in direct proportion to the pre-hole diameter. The specimen with a 10 mm hole diameter exhibited a maximum stroke of 2.9 mm. Analysis of the load–displacement curves revealed that larger diameters resulted in a shallower slope, indicating higher deformation capacity and energy absorption; specifically, these joints are capable of absorbing substantial energy before total failure. Conversely, the smallest diameters exhibited the steepest slopes, where higher joint stiffness led to separation at significantly shorter strokes. Although the peak tensile load was achieved

at a 9 mm diameter, the results for all pre-holed specimens remained higher than those of forge joining in terms of both maximum load and displacement.

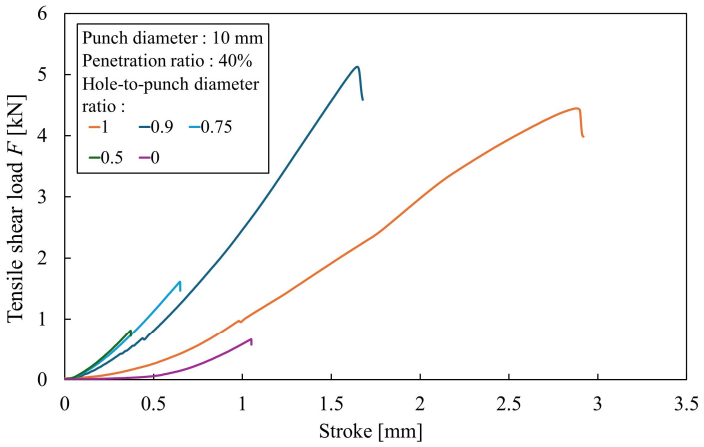


Figure 12. Load–stroke curves for specimens joined with different pre-hole diameters.

The press load generated during the forming process was also investigated, with the objective of reducing the forming load to improve energy efficiency. Figure 13 displays the press load profiles recorded after the initiation of the pressing cycle. The load spiked upon punch contact, reaching its peak almost immediately. Thereafter, a clear reduction in the peak press load was observed as the pre-hole diameter increased. Furthermore, although the nominal penetration ratio was set at 60%, the actual penetration achieved was lower due to the elastic deflection of the forming tooling and the press system under high loads. However, as detailed in Table 3, this actual penetration ratio increased in proportion to the pre-hole diameter. Specifically, while a pre-hole diameter of 7.5 mm yielded an actual penetration of only 43.9%, increasing the pre-hole diameter to 10 mm improved the actual penetration to 50.4%. It is inferred that a larger pre-hole facilitates smoother material flow, which significantly reduces deformation resistance. This reduction in resistance not only lowers the required press load but also minimizes tooling deflection, which dropped significantly from 46.7% to 16.0%, thereby allowing the punch to achieve a penetration depth closer to the nominal target. In contrast, the condition of no hole with an offset exhibited the highest tool deflection, reducing the actual penetration ratio to 32.0%. Although forge joining is easier to implement in manufacturing, it results in reduced energy efficiency. Notably, the forming load reached approximately 70 kN, which accelerates punch wear and potentially shortens tool life in long-term production.

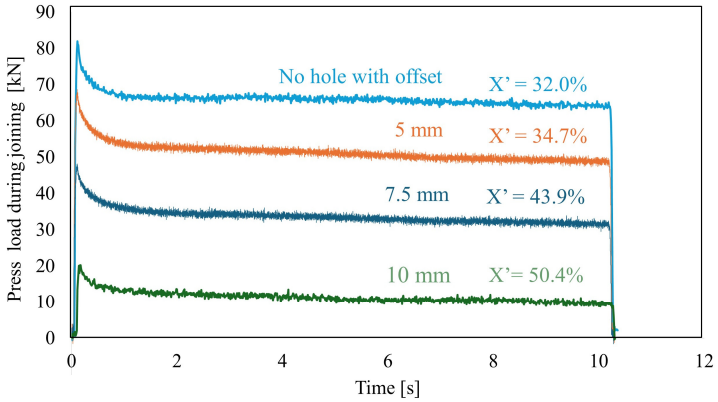


Figure 13. Press load characteristics for specimens with different pre-hole diameters.

Table 3. Effect of pre-hole diameter on actual penetration ratio and tool deflection. (Nominal penetration ratio = 60.0%).

Hole Diameter (mm)	No Hole with Offset	5	7.5	10
Actual penetration ratio (%)	32.0	34.7	43.9	50.4
Relative deviation (%)	46.7	42.2	26.8	16.0

While tensile shear tests evaluate the joint's resistance to in-plane forces, evaluating performance in a single loading direction is insufficient. Therefore, cross-tension tests were also conducted to assess the joint's resistance against loads applied perpendicular to the sheet plane. The cross-tension load capacities of the joints are presented in Figures 14 and 15. When comparing the two methods, forge joining with offset using a 10 mm punch without a pre-hole yielded a severely limited cross-tension load, peaking at merely 0.08 kN. In contrast, the pre-holed hot clinching method significantly outperformed the forge joining process; even with a minimal pre-hole diameter of 5 mm, the load nearly doubled to 0.15 kN. Furthermore, the load-bearing capacity of the joints increased consistently with the pre-hole diameter, reaching 0.54 kN at 7.5 mm and achieving a maximum of 0.77 kN at 10 mm. Although the cross-tension loads remained inherently lower than the tensile shear loads across all specimens, the pre-holed hot clinching method consistently delivered superior performance compared to forge joining under both loading conditions. To comprehensively evaluate the reliability of these joints under dynamic conditions, the fatigue performance warrants investigation in future studies.

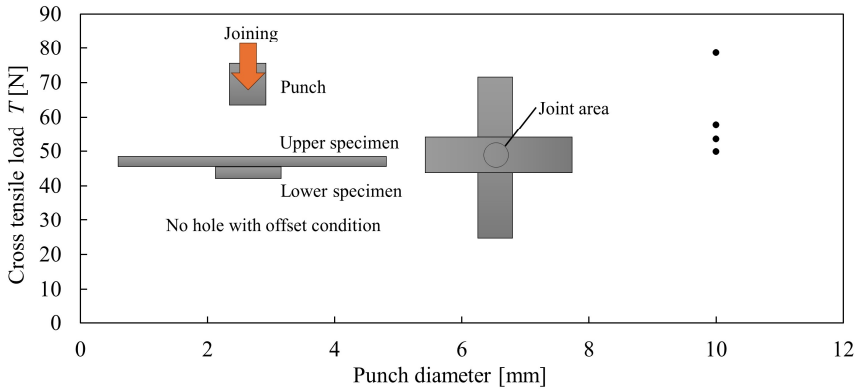


Figure 14. Relationship between cross-tension load and punch diameter for no hole with offset condition.

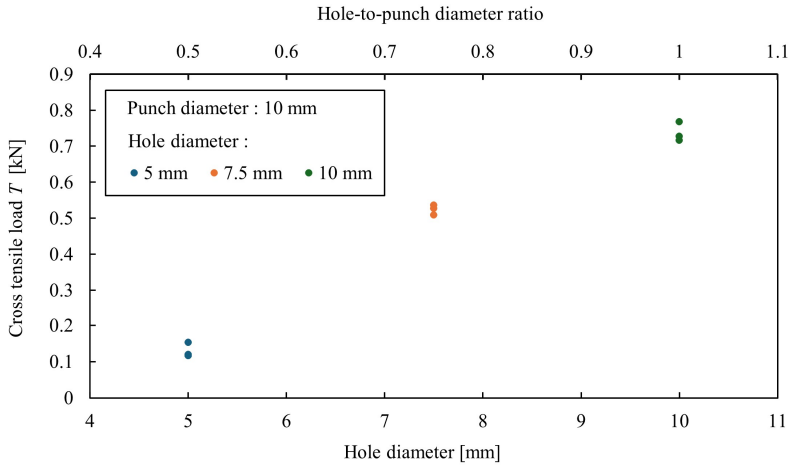


Figure 15. Relationship between cross-tension load and pre-hole diameter for pre-holed hot clinching.

The effect of a constant hole-to-punch diameter ratio was also investigated. Building upon the previous analysis of varying hole diameters with a constant punch size, this subsequent experiment maintained a fixed diameter ratio of 0.8. Specifically, punch diameters of 6.25, 7.5, 8.75, and 10 mm were paired with corresponding pre-hole diameters of 5, 6, 7, and 8 mm, respectively. By keeping the clearance constant and the nominal penetration ratio set at 60%, this study aimed to evaluate the relationship between the tensile shear load capacity and the proportional scaling of the tooling and hole dimensions.

As illustrated in Figure 16, the experimental results reveal a linear relationship between the joint load-bearing capacity and the simultaneous scaling of the punch and hole diameters, provided the diameter ratio remains constant. This linear enhancement is primarily attributed to the proportional expansion of the joint's circumferential shear area and the material volume within the pre-hole cavity. Specifically, the extended circumference linearly increases the primary shear-resisting area at the neck, distributing the applied stress more effectively. Simultaneously, the greater volume of material extruded into the pre-hole provides a higher resistance against shear failures. This linear proportionality contrasts with the behavior observed when varying only the hole diameter against a fixed punch size, which typically exhibits a non-linear trend during the optimization phase. In conclusion, while the hole-to-punch diameter ratio was optimized at 0.9, the overall tensile shear capacity of the joint can be systematically increased by proportionally scaling up both the punch and hole diameters. However, in practical applications, this upward scaling is inherently bounded by the available flange width of the tool components and the load capacity of the press equipment.

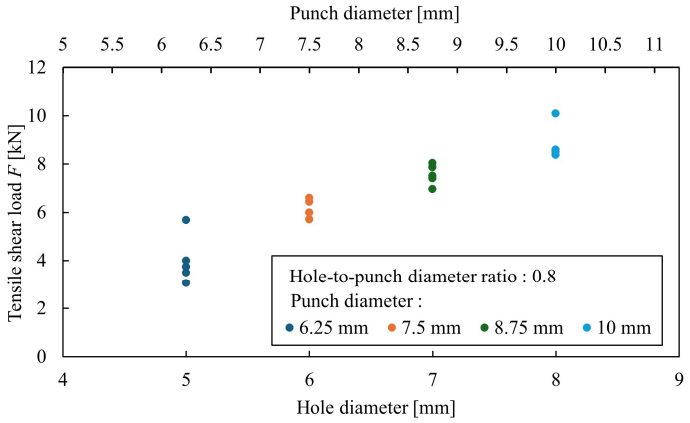


Figure 16. Relationship between tensile shear load and pre-hole diameter for hot clinching with a constant hole-to-punch diameter ratio.

3.2. Effect of Penetration Ratio on Joint Strength

In pre-holed hot clinching, the joint is formed by driving the upper and lower sheets into a flat die using a punch. The cavity within the lower sheet's pre-hole functions to guide and shape the material flow. As the material is compressed between the corners of the punch and the flat die, it flows radially outward to create a mechanical hook, which secures the sheets together. Precise control of the penetration ratio or punch stroke is essential because it governs the strain hardening and residual stress profile of the material. Since there is no geometric undercut to provide strength, the integrity of the joint or the modified material zone relies entirely on the localized thinning and the densification of the metal. If the penetration is too low, the material does not fill the cavity, resulting in insufficient bonding or shaping; conversely, excessive penetration leads to extreme thinning and formability limits, which can cause micro-fracturing or localized necking. Therefore, the penetration ratio serves as the primary metric to ensure that the material has been

sufficiently worked to achieve the desired mechanical properties without exceeding the material plastic deformation limits.

To evaluate joint performance, the effect of the penetration ratio of the sheet thickness on the tensile shear load was investigated. In these tests, the punch stroke was controlled based on the target initial percent penetration. The penetration ratio was set at 40%, 50%, 60%, and 70%, while pre-hole diameters of 5 mm, 7.5 mm, and 9 mm were studied to optimize the value of the tensile shear strength. The maximum tensile shear loads and the corresponding stroke curves obtained from the tension shear tests are presented in Figure 17. For every pre-hole diameter, the tensile shear load increases significantly with the punch penetration ratio. The load begins to rise at a 40% ratio, continues through 50%, and peaks at 60%. Specifically, the 7.5 mm pre-hole diameter achieved a maximum load range of 8.5–10.5 kN at this peak. Subsequently, at a 70% penetration ratio, the tensile shear strength declines. The load rose from 40% and dropped at 70%. A similar trend is observed for a hole-to-punch diameter ratio of 0.9, where the maximum tensile shear load reaches 9.5–11.5 kN at 60% penetration. This indicates that 60% represents the optimal penetration depth for material flow and densification in this configuration. While the pre-hole diameter also affects the magnitude of the load, with the 9 mm diameter yielding higher results than the 7.5 mm diameter and the 7.5 mm diameter yielding higher results than the 5 mm diameter, the gap between the 9 mm and 7.5 mm results is notably smaller. Despite these variations in magnitude, the fundamental behavior of the strength curve remains governed by the penetration ratio. Specifically, even at the optimized 0.9 ratio, the highest strength is achieved only when penetration is maintained at the 60% threshold.

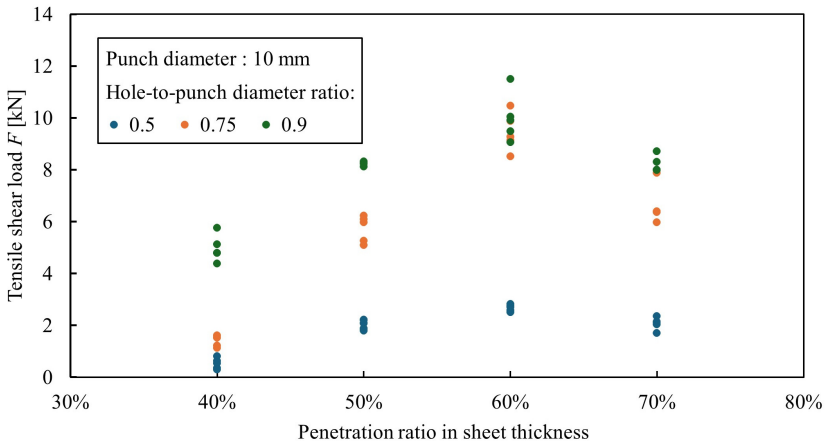


Figure 17. Relationship between maximum tensile shear load and penetration ratio for specimens with pre-hole diameters of 5 mm, 7.5 mm, and 9 mm.

The tensile shear load–stroke curves for joints with a hole-to-punch diameter ratio of 0.9 are presented in Figure 18. The data indicate that joints sharing the same hole-to-punch ratio exhibit a similar slope regardless of the penetration ratio, suggesting that the initial stiffness of the joints remains consistent. However, the total stroke at failure varies significantly with the penetration ratio. The 60% penetration ratio achieved the highest displacement, reaching a stroke of 3.5 mm before failure. In comparison, the 50% and 70% penetration levels showed similar displacement behavior, both failing at approximately 2.5 mm. The 40% penetration ratio resulted in the lowest performance, which yielded both the minimum tensile strength and the shortest stroke of 1.7 mm. These results indicate a direct correlation between joint quality and energy absorption; the optimized joint (60% penetration) was characterized by both a higher peak load and a significantly larger stroke, suggesting superior ductility and overall toughness.

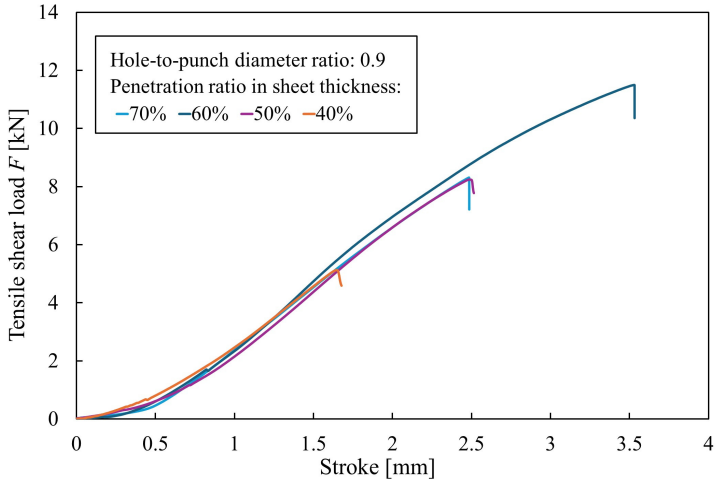


Figure 18. Load–stroke curves for specimens joined with different penetration ratios.

3.3. Failure Mode

Two distinct failure modes were identified in the pre-holed hot clinched joints during tensile shear testing: neck fracture and button separation. Figure 19 illustrates the failure modes, with Figure 19a. showing a primary button separation (pull-off failure), and Figure 19b exhibits a neck fracture (neck-break failure) mode detailing the specific characteristics of each mode. Additionally, Figure 20 shows a photograph of each mode.

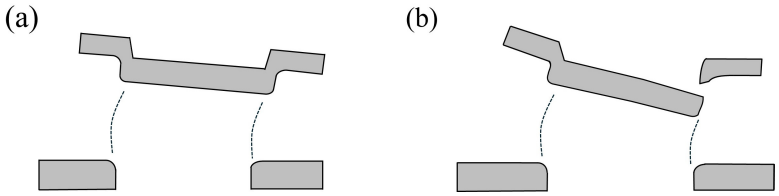


Figure 19. Fracture mode of specimen: (**a**) button separation mode and (**b**) neck fracture mode.

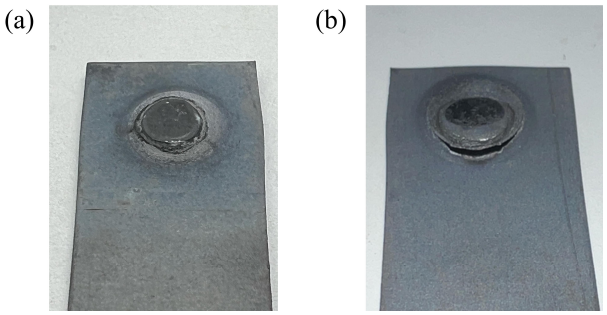


Figure 20. Photographs of failure modes in the upper specimen: (**a**) button separation and (**b**) neck fracture.

The term "button separation" refers to the complete removal of the joint from the lower sheet, resulting in a specimen with minimal fracture area. In contrast, "neck fracture" describes a scenario where the upper sheet's joint is pulled from the lower sheet, accompanied by a fracture of the upper sheet. The occurrence of button separation mode is attributed to an insufficient penetration ratio of the joints, whereas neck fracture results from a sufficient penetration ratio, which ultimately leads to fracture of the joint's neck.

The failure modes of the joints in Figure 20b, particularly the neck fracture mode, show instances where the upper specimen undergoes sudden material tearing, leaving a hole at the joint neck location. This failure mode demonstrates a high degree of correlation with the optimal joining parameters. Notably, all joints exhibiting neck fracture achieved a very high

maximum tensile shear load, evidencing an effective joint. Neck fracture was consistently observed at a hole-to-punch ratio of 0.9 across penetration ratios of 50%, 60%, and 70%. However, at a ratio of 0.75, this failure mode occurred only at 60% penetration, and at a 0.8 ratio, nearly all specimens exhibited neck fracture at 60% penetration. In summary, at a 60% penetration ratio, a hole-to-punch diameter ratio of 0.75 or higher resulted in neck fracture for almost all specimens; otherwise, the failure transitioned to the button separation mode, which included all cross-tension test specimens.

4. Experimental Validation of Quenching in the Punch Compression Zone and the Surrounding Surface Area

The fractures and localized failures are frequently observed in conventional thermally assisted clinching, often attributed to inhomogeneous hardness resulting from non-uniform heating [23]. Therefore, precise control of the cooling process is critical to improving the overall joint condition. Furthermore, while integrating clinching into the hot stamping cycle addresses ductility constraints, maintaining thermal uniformity remains a critical challenge. The process is highly sensitive to the material interface; specifically, uneven contact or gaps between sheets cause current concentration and non-uniform heating. The overlapping sheets of patchwork blanks create a localized increase in thermal mass, leading to temperature gradients between the reinforcement and the base sheet.

This non-uniformity can result in inconsistent material flow and, more importantly, variations in the cooling rate. As reported in [23], conventional thermally assisted clinching, if the quenching rate in the thickened joint area falls below the critical threshold, the martensitic transformation may be incomplete, resulting in soft zones that compromise the structural integrity of the component. This weakness often causes the surrounding material to fracture during shear testing before the interlock itself fails. To solve these issues, a pre-holed lower specimen is utilized to define joint geometry, replacing the conventional die cavity. This approach effectively allows for the use of a flat die, thereby simplifying the tooling interface and improving thermal contact. By focusing on the cooling process and optimizing the material flow through this pre-holed configuration, we aim to achieve more uniform mechanical properties throughout the joint. To confirm the efficacy of this method, a thermocouple was spot-welded at the center of the punch compression zone to precisely record the specimen's thermal history, as illustrated in Figure 21.

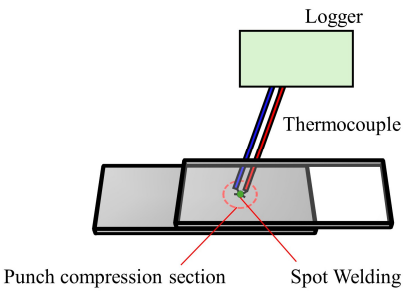


Figure 21. Schematic of thermocouple placement for temperature measurement at the center of the punch compression zone.

The resulting temperature profile is presented in Figure 22a. Upon initiation of heating, the specimen reached the target temperature of 950 °C after approximately 200 s. This peak temperature is significantly above the Ac_3 transformation temperature at 863 °C [36], ensuring a complete austenitic transformation. The subsequent holding period facilitated the diffusion of aluminum into the base metal. Following the heating phase, the specimen was removed from the furnace and transferred to the die for the joining process. Following furnace removal, the specimen was transferred to the die with a 5 s interval

before the punch made contact, during which the temperature dropped to approximately 850 °C. Subsequently, a 10 s die-quenching period reduced the specimen temperature to approximately 170 °C. The martensite start and finish temperatures were around 396 °C and 210 °C [36], respectively. As illustrated in Figure 22b, the transition from the start of cooling to the completion of martensite formation occurred over a total duration of 6 s. The resulting average cooling rate of 107 °C/s significantly exceeded the material's critical cooling rate of 30 °C/s [4], confirming that the process parameters are sufficient to achieve a fully martensitic transformation and high hardness properties in the joint.

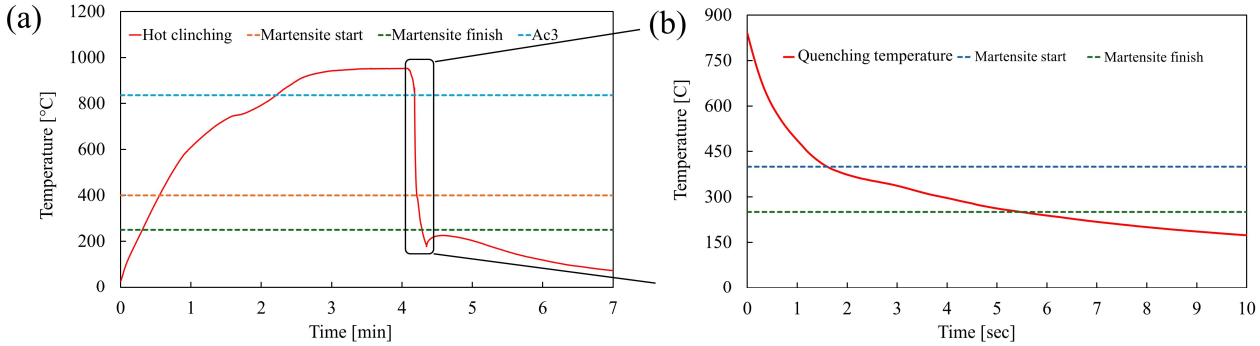


Figure 22. Temperature history in the center of the punch compression section: (**a**) time from heating start and (**b**) time from stamping.

4.1. Hardness Distribution of Joint Area

The micro-Vickers hardness was investigated on the joint cross-sections to verify the quenching effect within the joint zone. For the evaluation, specimens of both pre-holed hot clinching and forge joining methods were cut and embedded in resin. The compression and penetration ratios were set at 60%, with a pre-hole diameter of 9 mm, and the punch diameter was 10 mm for both experiments. The hardness measurement positions are illustrated in Figure 23a,b. The hardness testing was performed using a micro-Vickers tester across specific regions to map the material properties. To ensure statistical reliability, each test was conducted five times, and the average value was used as the test result, as shown in Table 4a,b. The upper specimen was tested at multiple positions across both its upper and lower regions to capture the full hardness profile. For the lower specimen, measurements were concentrated in the lower region to evaluate the quenching effect near the tool-contact surface. This comparative analysis allows for the validation of the martensitic transformation across both joining methods.

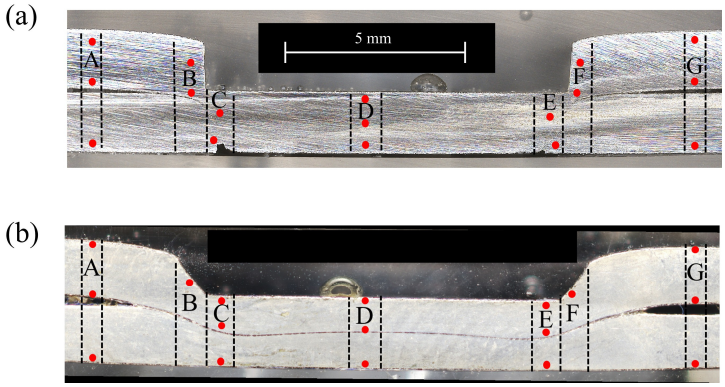


Figure 23. Vickers hardness measurement locations on the cross-section of the die quenched joint: (**a**) pre-holed hot clinching and (**b**) forge joining.

Table 4. Vickers hardness distribution across the measured positions on the cross-section of the die quenched joint: (a) pre-holed hot clinching and (b) forge joining [Unit: HV].

(a)							
Pre-holed hot clinching	A	B	C	D	E	F	G
Top of upper specimen	500 ± 19	504 ± 9		544 ± 16		509 ± 10	489 ± 20
Bottom of upper specimen	496 ± 18	527 ± 10	537 ± 17	537 ± 19	534 ± 13	531 ± 9	499 ± 19
Bottom of lower specimen	545 ± 3		541 ± 9		543 ± 13		534 ± 13
(b)							
Forge joining	A	B	C	D	E	F	G
Top of upper specimen	450 ± 11	474 ± 3	460 ± 9	526 ± 3	445 ± 12	466 ± 16	453 ± 10
Bottom of upper specimen	478 ± 11		471 ± 12	529 ± 13	514 ± 6		473 ± 8
Bottom of lower specimen	471 ± 2		500 ± 6	534 ± 8	514 ± 18		462 ± 5

Cross-sectional observations of the specimen, cut along the width direction at the center of the circular punch compressed region, are presented in Table 4a,b. The results indicate that hardness across all measured zones exceeded 450 HV, surpassing the critical Vickers hardness threshold for martensite [36]. The observed hardness exceeding 500 HV at the central part was primarily driven by ausforming during the hot stamping process [37,38]. While standard fully martensitic 22MnB5 steel yields a base hardness of ~450 HV, the severe plastic deformation induced by the punch, which improved the compression and penetration ratios, combined with holding it at bottom dead center until martensitic transformation was complete, effectively promoted this ausforming mechanism. This process refined the microstructure and leveraged volume expansion during the phase change, thereby significantly increasing the quenched hardness of locally compressed areas. Since both ends were hardened solely by die contact without undergoing this ausforming process, they exhibited relatively lower hardness values. Furthermore, across all measurement positions, the lower part of the lower specimen consistently showed higher hardness than the upper part of the upper specimen, which can be attributed to the superior heat transfer at the lower die side.

When comparing the two methods, pre-holed hot clinching exhibited a higher hardness distribution than forge joining across all measured areas. This increase was primarily attributed to pre-holed hot clinching inducing a greater degree of large plastic deformation, which consequently amplified the ausforming effect and strain hardening, combined with a reduced volume of material to be quenched. As illustrated in Table 4a, the hardness distribution for pre-holed hot clinching peaked in the middle area of the upper specimen at location D, where the average hardness measurements were 544 HV and 537 HV, respectively. Conversely, the upper regions of the upper specimen at locations A and G showed lower hardness, averaging 500 HV and 489 HV, respectively, because the material had lost contact with the upper die during quenching, preventing consistent hardening. Furthermore, the central regions, locations B and F of the upper specimen, located around the punch edge, were critical zones where fractures typically occurred during tensile shear testing. This was because significant stress concentrations occurred at these edges, where insufficient hardness or material thinning can critically reduce the overall joint strength.

4.2. Microstructure Analysis

The microstructures were examined. After polishing the cross-section, it was etched for about 5 s with Nital solution (97% ethanol, 3% nitric acid) and then washed with ethanol. Subsequently, microstructural observation was performed using an optical microscope. Figure 24 shows the microstructures obtained at each measurement location. The results

primarily exhibited a mixed microstructure of martensite and bainite. This microstructural composition was consistent with the measured hardness values and the thermal history of the process. The grain size was fine overall, although some areas with coarsened grains were also observed.

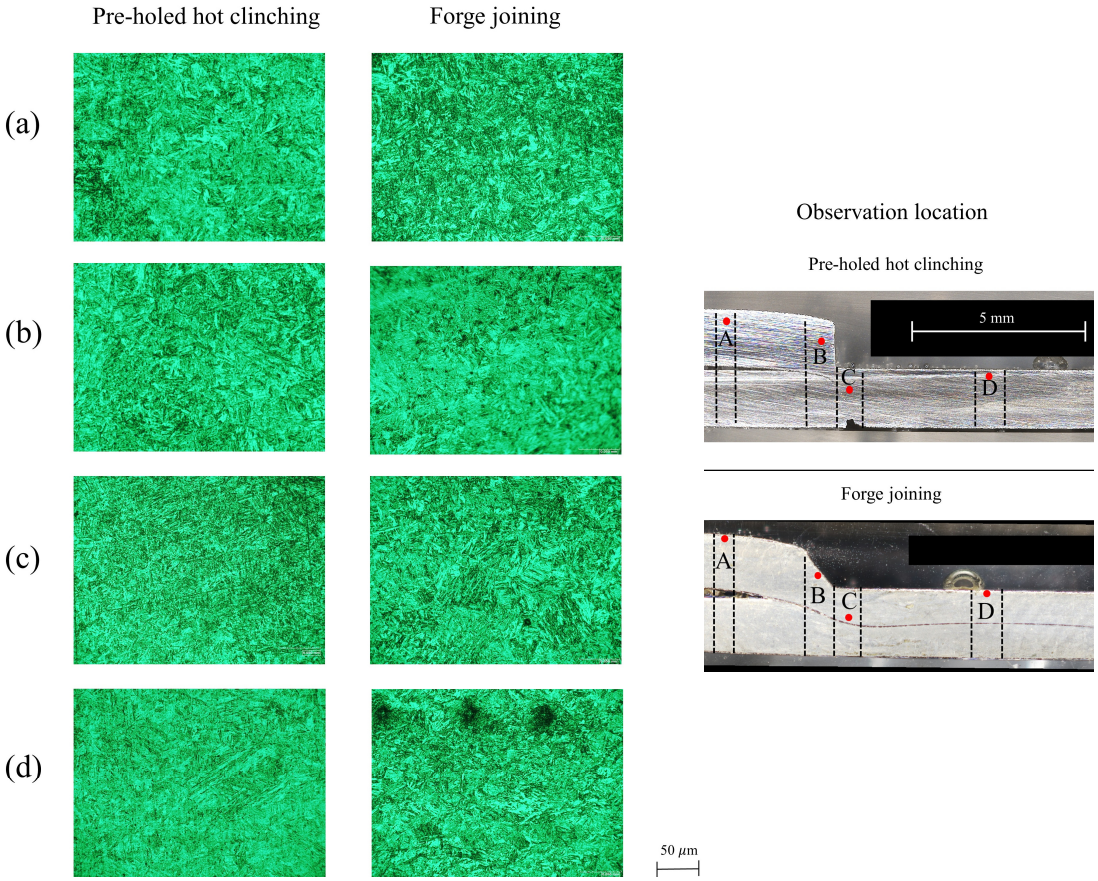


Figure 24. Microstructure of each measurement position between pre-holed hot clinching and forge joining according to location in Table 4: (**a**) top of upper specimen (location A); (**b**) top of upper specimen (location B); (**c**) bottom of upper specimen (location C); and (**d**) top of upper specimen (location D).

While both processes benefit from the ausforming effect during plastic deformation, pre-holed hot clinching exhibited a higher hardness distribution than that of forge joining across the entire joint area. This superior hardness was attributed to the greater degree of plastic deformation induced by pre-holed hot clinching, which consequently amplified the ausforming effect. As shown in Figure 24, the microstructure mainly consisted of acicular martensite with some localized coarsened grains, suggesting that the high plastic flow driven by this enhanced ausforming helped refine the grains and improved overall joint strength. The presence of acicular (needle-like) martensite was a result of the rapid cooling or quenching from the high temperatures reached during the pre-holed hot clinching process. As shown in the microstructural comparison in Figure 24a, the forge joining method exhibited partially insufficient quenching. Specifically, the forge-joining region consisted of a mixed microstructure of martensite and bainite, which is consistent with the lower hardness value of 450 ± 11 HV. Furthermore, the presence of retained austenite was considered negligible due to the high cooling rates and was not discernible under optical microscopy. In contrast, the pre-holed hot clinching method produced a finer grain structure, indicating a higher volume fraction of martensite with a hardness of 500 HV. As shown in Figure 24c,d, both methods achieved a finer martensitic structure due to

ausforming; however, the amplified ausforming effect in pre-holed hot clinching was particularly evident in Figure 24c, where hardness values reached 537 HV, compared to 471 HV for forge joining. This evidence suggested a corresponding improvement in the overall tensile shear strength of the pre-holed hot clinching joints.

Upon closer inspection, as shown in Figure 25, the results reveal that the pre-holed hot clinching method produced bonding interfaces where the parent phases of the upper and lower specimens were joined. The analysis confirmed that solid-state bonding is one of the primary mechanisms responsible for interfacial adhesion. As a result, most areas were connected through an alloy layer, which is consistent with the phenomenon observed in the forge joining method.

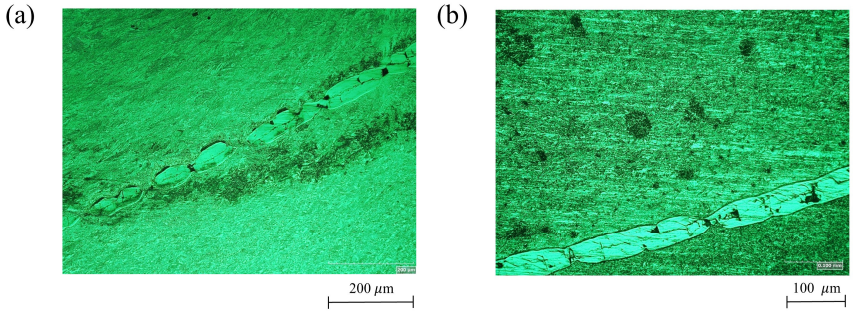


Figure 25. Solid-state bonding at the interface of the upper and lower specimens: (**a**) pre-holed hot clinching and (**b**) forge joining.

This process involves extruding surface contaminants that hinder bonding, such as oxide films, through friction and plastic deformation. This action allows for the formation of metallic bonds as active atoms are exposed on the bonding surface. Consequently, this study confirmed instances of adhesion between the base metals where the original joint interface disappeared entirely, indicating a superior metallurgical bond.

Building upon this mechanism, the presence of the pre-hole plays a critical role in differentiating the joint strength from that of conventional forge joining. In the conventional process, relatively uniform surface expansion limits bonding primarily to the weaker Al–Si coating layers. In contrast, the pre-holed configuration actively facilitates profound interfacial cleansing. During forming, the edge of the lower sheet's pre-hole induces severe localized surface expansion. This intense deformation drags and segments the brittle Al–Si coating, causing it to fracture and expose the newly formed surfaces of the underlying steel substrate. By joining these base metal surfaces directly together within the micro-gaps, the pre-holed process achieves a solid-state bond that is fundamentally stronger than the coating-dominated adhesion observed in conventional forge joining.

This phenomenon explains the presence of cross-tension strength even in the absence of a mechanical interlock between the specimens. However, forge joining lacks a geometric hook, which results in poor ductility and leads to brittle fracture during deformation. Consequently, the combination of mechanical joining and localized solid-state bonding in pre-holed hot clinching significantly enhances joint strength. This hybrid mechanism allows the joint to achieve high performance without relying solely on the mechanical interlock typical of conventional clinching.

4.3. Effect of Gap Size on the Surface Hardness Distribution Within the Surrounding Joint Area of the Specimen

The surface hardness distribution was investigated to confirm the hardening in regions beyond the joint area. The primary objective of the quenching process is to ensure a uniform hardness distribution across the entire sheet, thereby preventing crack initiation and fracture. As illustrated in Figure 26, the application of a reinforcement sheet to a base

sheet in a patchwork blank created a gap between the specimen and the die. The maximum allowable gap for maintaining required material properties was investigated. The gap length between the specimen edge and the die varied at 2 mm, 10 mm, and 20 mm.

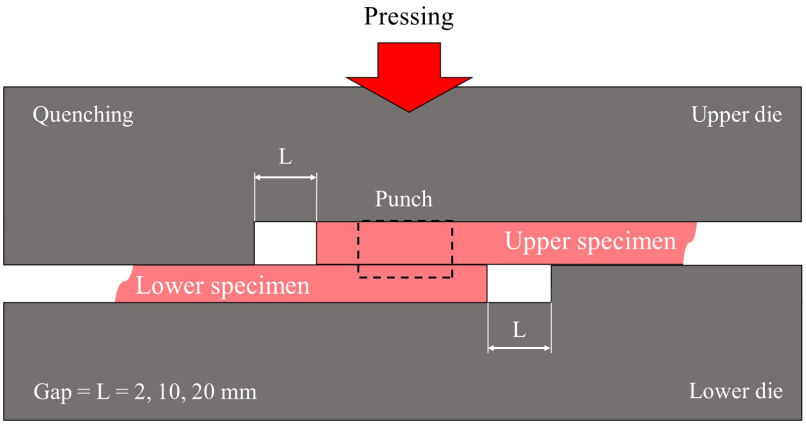


Figure 26. Illustration of the gap between the specimens and die surface during pre-holed hot clinching process.

Following the separation of the joined specimens at a 60% penetration ratio, the entire surface was polished to prepare for Vickers hardness testing. As illustrated in Figure 27, measurement positions were fixed at the center of the specimen width. In the longitudinal direction, measurements were taken at 5 mm intervals, beginning at a distance of 10 mm from the punch center (defined as 0 mm). Given the specimen lengths of 70 mm for the upper specimen and 90 mm for the lower specimen, hardness was recorded at five and six locations, respectively. Testing was conducted on both the top and bottom surfaces, with 5 measurements performed at each location to determine the average hardness value.

Figure 27 illustrates the hardness distribution from the experimental results, where the horizontal axis denotes the distance from the starting point and the vertical axis represents the Vickers hardness. At a measurement distance of 0 mm, the Vickers hardness exceeds 500 HV across all tested conditions. This observation aligns with the hardness data obtained from the cross-section as shown in Table 4.

The hardness distribution of the specimen surfaces was highly sensitive to the die gap, as evidenced by the variations observed across the 2 mm, 10 mm, and 20 mm gap configurations. As illustrated in Figure 27a,b, the hardness profiles of the lower specimen's top surface and the upper specimen's bottom surface, for the 20 mm gap, exhibited a local minimum of approximately 448 HV at the 15 mm measurement distance, falling slightly below the 450 HV martensitic transformation threshold. This degradation in properties is attributed to the transition from conductive die quenching to convective air cooling within the gap, particularly in regions where the specimen surface fails to maintain contact with the die. However, the hardness recovered at the 20 mm and 25 mm measurement distances, reaching levels consistent with the 2 mm gap configuration. In comparison, the 10 mm gap showed a hardness reduction from the 0 mm reference to a minimum of 488 HV at the 10 mm measuring distance. Conversely, the 2 mm gap representing a near-zero clearance maintained a hardness exceeding 500 HV across all distances with a peak of 550 HV, demonstrating uniform quenching. Furthermore, the opposite surfaces, as shown in Figure 27c,d, the hardness values reached their minimum at both the 5 mm and 10 mm measurement distances. Specifically, the bottom surface of the lower specimen and the top surface of the upper specimen exhibited lower hardness of approximately 500 HV and 480 HV, respectively. The absence of interfacial contact between the die and the opposing surface of the specimen limits the heat transfer, resulting in the obtained hardness reduction.

Experimental findings indicate that a gap of up to 10 mm is the optimal parameter for maximizing surface hardness and ensuring a uniform metallurgical transformation.

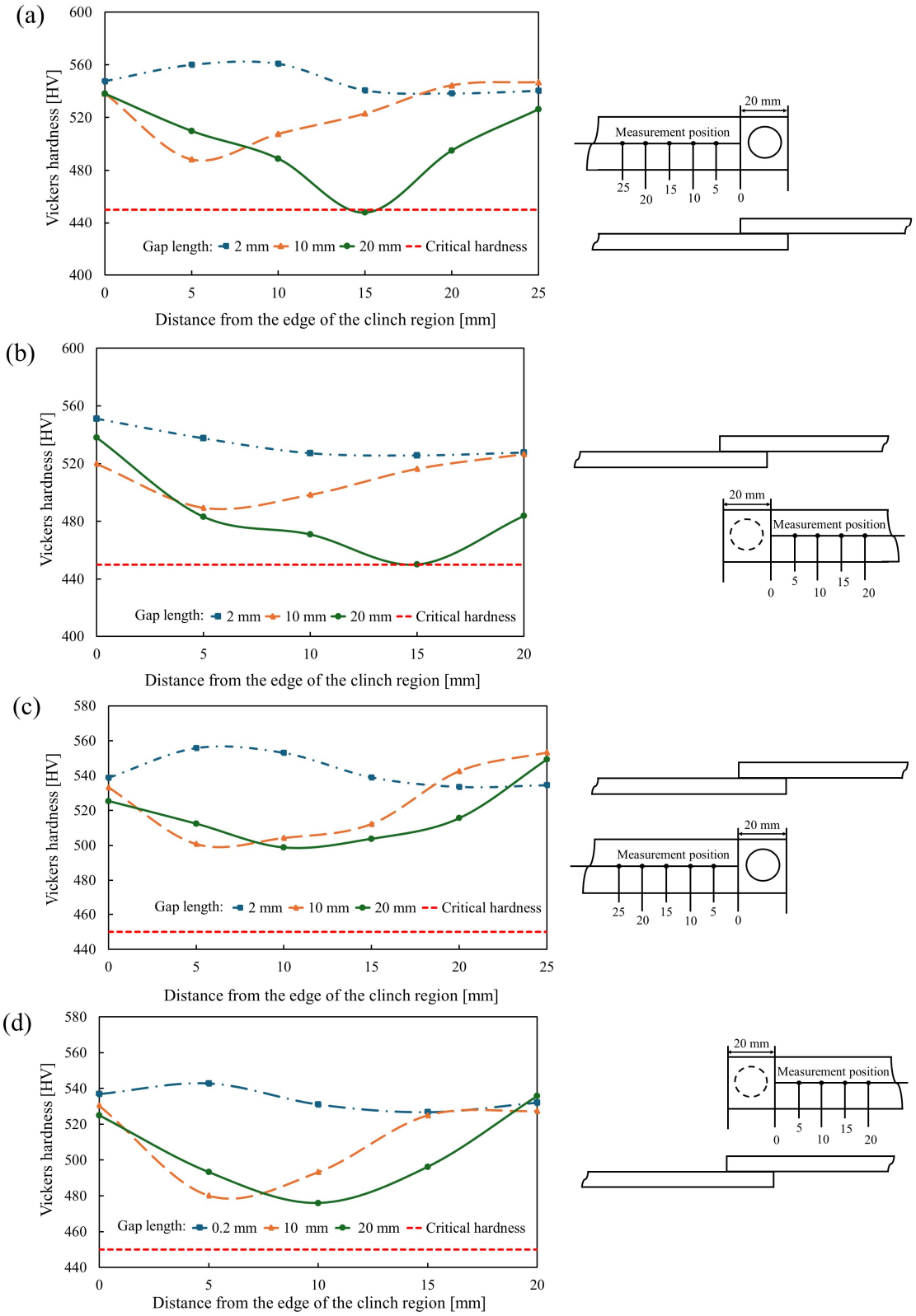


Figure 27. Vickers hardness values at specified measurement positions: (**a**) lower specimen at top surface; (**b**) upper specimen at bottom surface; (**c**) lower specimen at bottom surface; and (**d**) upper specimen at top surface.

5. Analysis of the Joining Mechanism in Pre-Holed Hot Clinching Using Finite Element Analysis

Experimental results demonstrated that pre-holed hot clinching provided significantly higher strength than forge joining in both tensile shear and cross-tension testing, despite the absence of a mechanical interlock. Microstructural analysis revealed that while a solid-state bonding mechanism occurred in both processes, pre-holed hot clinching exhibited a substantial increase in joint strength, prompting a detailed investigation into the underlying causes of this improvement. To capture the bonding mechanism as the upper specimen flows into the pre-hole, a dual methodology was employed using experimental cross-sections and Finite Element Analysis (FEA), utilizing the same simulation conditions as the reference study [27], to evaluate material movement through effective plastic strain. The investigation identified the highest tensile shear strength by varying the penetration ratio (30–70%) using a 9 mm pre-hole diameter and a 10 mm punch.

The study utilized surface expansion rate and contact pressure distributions at a 60% penetration ratio to compare pre-hole diameters of 5 mm, 9 mm, and 12.5 mm against a constant 10 mm punch diameter. These metrics explain how the pre-hole configuration enhances bond strength in hot stamping applications far beyond the capabilities of solid-state bonding. The integration of pre-hole geometry not only prevents material fracturing or necking during the forming of ultra-high-strength steel but also activates a solid-state bond through optimized surface expansion rate and contact pressure.

The correlation between the Finite Element Analysis (FEA) results and the experimental cross-sections demonstrates a highly consistent material flow pattern across the entire range of investigated penetration ratios (30–70%), as shown in Figure 28. While the FEA model provided a comprehensive, full-scale visualization of the effective plastic strain across the entire joint, the experimental validation focused specifically on the corner region to provide a high-resolution, microscopic comparison of the most critical deformation zone. This localized analysis of the punch corner is essential, as this specific region is where the most severe shearing and material stretching occur, directly influencing the final joint strength. It is within this critical zone that the dual joining mechanism is established: the formation of a solid-state bond along the interface and a mechanical hook derived from the resulting geometric shape.

The simulated strain distribution effectively captured the localized deformation behavior observed in the physical specimens, with peak strain intensities shifting from the immediate punch corners at lower penetration levels toward the neck region as the penetration ratio increased. The bonding mechanism is primarily driven by the interfacial slipping of the upper specimen as it flows into the lower pre-hole. As the upper material was forced into the cavity, the rigid walls of the lower specimen created a dragging effect along the interface, which significantly enhanced the surface expansion rate. This phenomenon of intense contact not only cleans the contact surfaces by breaking down oxide layers but also facilitates the exposure of fresh metal atoms.

As the penetration ratio increased to 50–60%, this dragging-induced expansion, combined with high contact pressure, transitioned the interface from a slipping state into a permanent solid-state bond. This localized mechanism explains the superior strength of the 9 mm hole configuration, where the tighter clearance optimizes the contact pressure and dragging force required to generate sufficient surface expansion for a high-integrity joint. As illustrated in Figure 28i, the unbonded region (indicated by the black areas) within the punch section diminished significantly at a 60% penetration ratio compared to other penetration ratios, signifying the development of solid-state bonding over a more extensive interface. It is inferred that the achievement of a broader bonding area under these specific conditions was a primary factor contributing to the substantial improvement

in joint strength. Moreover, the narrow clearance between the punch and the pre-hole promotes the formation of a mechanical bond between the upper and lower specimens. As the penetration ratio reached 60%, the upper material completely filled the die cavity, creating a geometric hook that significantly enhances joint strength. This mechanical bond leverages the high yield strength of the material, as the joint shape provides a physical constraint that supplements the solid-state bonding interface.

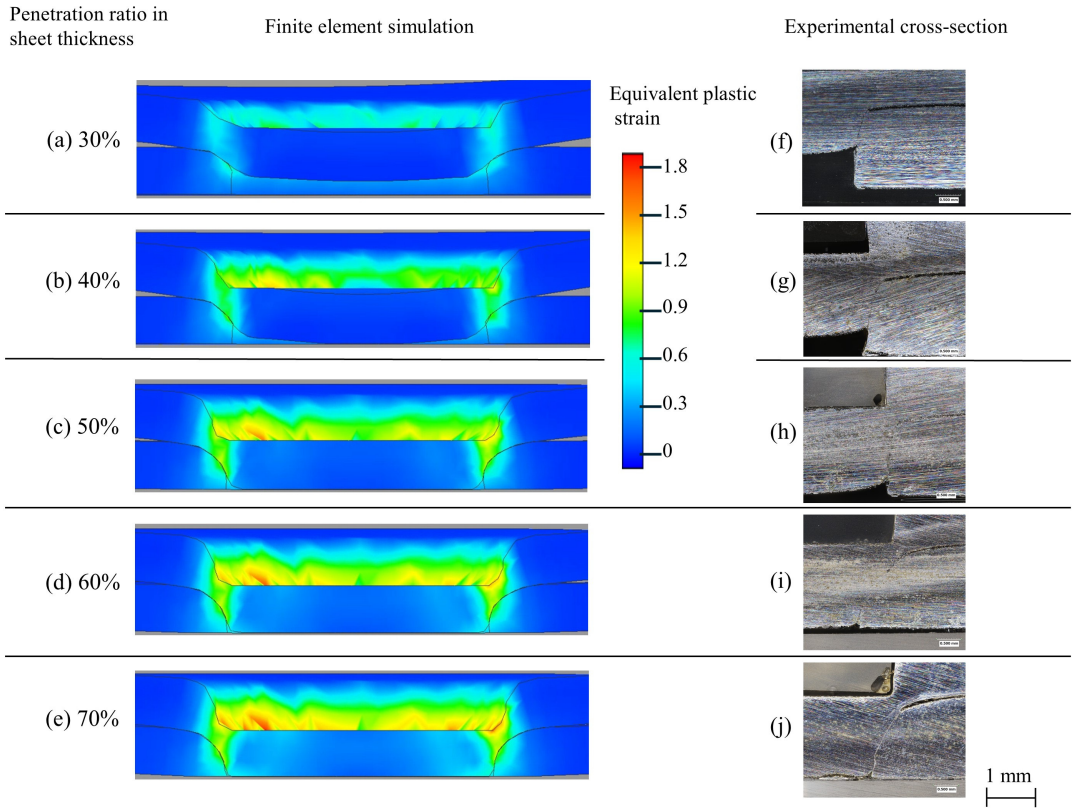


Figure 28. Comparison of central cross-sections between FEA simulation and experimental results at various penetration rates: (**a**–**e**) Equivalent plastic strain distribution from FEM (30–70% penetration) and (**f**–**j**) corresponding experimental cross-sections.

Fundamentally, as the penetration ratio increases, the necking region is subjected to higher equivalent plastic strain. This intense strain induces an ausforming effect, which promotes significant strain hardening, a finer grain microstructure, and increased hardness, thereby boosting the overall strength of the joint. However, once the penetration ratio increased to 70%, the joint integrity began to degrade. As illustrated in Figure 28j, the solid-state bonding interface tends to delaminate, while the necking region becomes excessively thin, significantly increasing the risk of premature rupture. Furthermore, as shown in Figure 28e, the extreme localized strain at this 70% depth amplified the ausforming and severe subsequent strain hardening effects to a detrimental level; the resulting exceptionally high hardness rendered the material excessively brittle. These combined factors, interfacial delamination, critical neck thinning, and strain-induced embrittlement, explain why the 70% penetration ratio resulted in a measurable reduction in joint strength compared to the optimal 60% ratio.

As illustrated in Figure 29b,e, a detailed analysis of the solid-state bonding interface revealed a significant disparity in the surface expansion rates between the two specimens. A substantial expansion rate was observed at the contact interface of the upper specimen, whereas the lower specimen remained largely static or decreased. Specifically, while the top surface of the lower specimen exhibited a localized increase in the expansion rate due to ini-

tial contact, the area along the vertical pre-hole walls showed a negligible surface expansion rate. This disparity confirmed the interfacial slipping phenomenon mentioned previously; the upper material was forced to slide and stretch against the rigid, non-deforming walls of the lower specimen. This localized dragging and intense surface expansion are the primary drivers for breaking down oxide layers, thereby facilitating the formation of a high-strength solid-state bond. Figure 30 shows that the surface expansion dynamics between the upper and lower specimens are highly dependent on the hole size. Under conditions with no hole, the specimens undergo complete integral deformation; despite the large data scattering, there is minimal difference in their maximum surface expansion rates. Specifically, the differential maximum surface expansion rate (the difference between the peak surface expansion rate of the upper and lower specimens) is only 27.2% for the 0 mm condition. This lack of relative slippage does not directly contribute to improved joint strength. A similar uniformity in expansion values is observed with a 5 mm hole, where the behavior between the two specimens remains largely indistinguishable, exhibiting a differential maximum surface expansion rate of 23.2%. However, as the hole size increases, a distinct shift occurs: the surface expansion rate of the upper specimen becomes significantly higher than that of the lower specimen. This discrepancy reaches its optimal value at a diameter of approximately 9 mm, where the differential maximum surface expansion rate significantly increases to 66.2%. Notably, interfacial slip is also most active at this specific dimension, suggesting that the relative slippage induced by larger holes plays a critical role in enhancing the overall joint strength. Beyond this optimal size, for hole diameters exceeding 10 mm, both the expansion rates and the discrepancy between the specimens begin to decrease, indicating a reduction in effective interfacial slip.

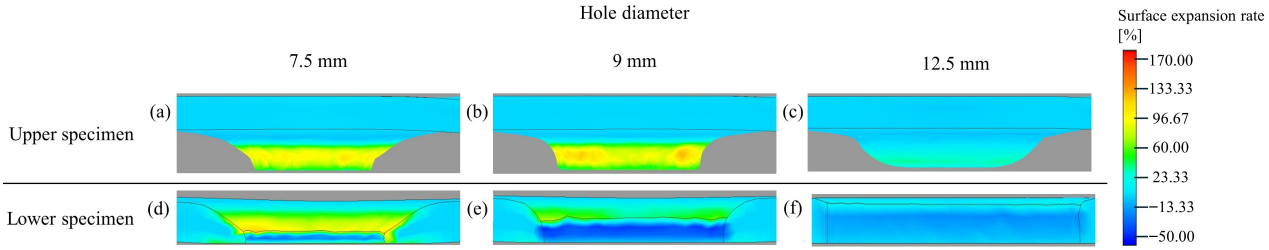


Figure 29. Distribution of surface expansion rates on the contact surfaces obtained from FEA simulation: (**a**–**c**) upper specimen and (**d**–**f**) corresponding lower specimen, evaluated at hole diameters of 7.5, 9, and 12.5 mm.

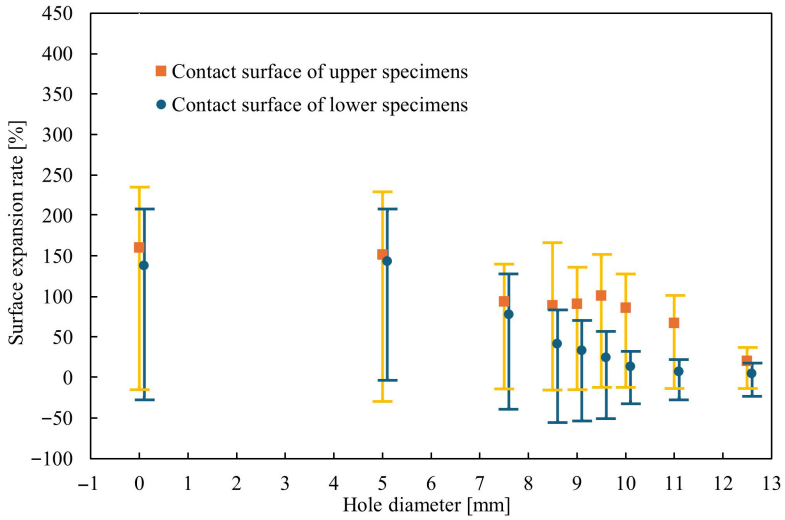


Figure 30. Comparison of surface expansion rates between upper and lower specimens as a function of pre-holed diameters.

Furthermore, as illustrated in Figure 31b,e, the distribution of contact pressure was predominantly higher at the interface of the upper specimen relative to the lower specimen. Despite this localized intensity, the pressure remained notably uniform across the critical joining zones. Specifically, significant contact pressures were maintained around the necking region and along the vertical side walls of the pre-hole. This widespread distribution of contact pressure indicates that solid-state bonding is extensively developed across these interfaces. When comparing these results to the 7.5 mm pre-hole diameter, as illustrated in Figure 29a,d, the interfacial slipping phenomenon was still present but occurred to a much lesser extent. While the top surface of the lower specimen exhibited a localized increase in the expansion rate due to initial contact and forming, the surface expansion along the extremely short vertical pre-hole walls remained negligible. This lack of sufficient vertical interface prevents the formation of an effective geometric shape, thereby limiting the potential for solid-state bonding. Furthermore, as shown in Figure 31a,d, the contact pressure distribution was notably non-uniform across both specimens. Unlike the 9 mm diameter, the contact pressure levels in the upper and lower specimens were nearly identical, suggesting that the material flow was overly constrained. These factors, poor geometric joint and insufficient interfacial expansion, explain the lower overall joint strength observed in the 7.5 mm configuration. In contrast, for the 12.5 mm pre-hole diameter, the contact pressure was virtually non-existent across both specimens, as illustrated in Figure 31c,f. This lack of contact pressure resulted from the fact that the volume of material displaced by the punch was significantly less than the total volume of the pre-hole. Consequently, the cavity remained incompletely filled, with material contact often occurring on only one side of the hole. This insufficient filling prevents the establishment of thorough interfacial contact, which is necessary to generate the normal force required for bonding.

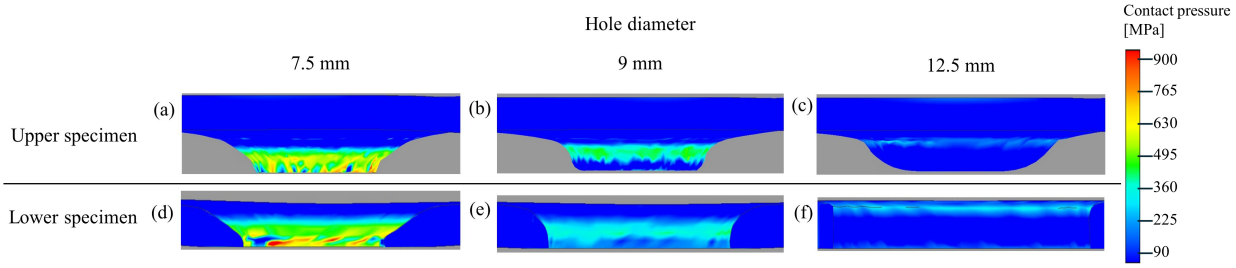


Figure 31. Distribution of contact pressure on the contact surfaces obtained from FEA simulation: (**a**–**c**) upper specimen and (**d**–**f**) corresponding lower specimen, evaluated at hole diameters of 7.5, 9, and 12.5 mm.

Furthermore, the surface expansion rate was observed only in the upper specimen, indicating a total absence of solid-state bonding at the interface. Without the material reaching the vertical walls of the hole, no geometric hook shape is formed, and no interfacial slipping occurs to clean the surfaces. The 12.5 mm configuration was inherently difficult to join, often resulting in no initial bonding. These combined deficiencies, the lack of mechanical interlock and the absence of a metallic bond explain the inadequate joint strength and the premature separation under load.

The mechanical coupling between contact pressure and the surface expansion rate constitutes the fundamental mechanism for establishing a high-strength solid-state bond within the optimized 60% penetration ratio. The high surface expansion rate in the upper specimen, particularly localized within the necking region, facilitates the breakdown of brittle oxide layers and the exposure of fresh metal atoms, while the rigid, non-deforming walls of the lower specimen induce an interfacial slipping phenomenon that enhances this "cleaning" effect through intense dragging. Simultaneously, the uniform contact pressure

distributed along the vertical side walls provides the necessary normal force to bring these nascent surfaces into intimate contact, enabling atomic-level bonding across a wider effective area.

This dual mechanism ensures that the upper material not only fills the pre-hole cavity to form a geometric anchor but also achieves a metallurgical connection. In larger pre-hole diameters, the lack of sufficient radial constraint leads to inadequate contact pressure and minimal interfacial stretching, which ultimately compromises joint integrity. Conversely, the 9 mm configuration provides the optimal constraint required to maximize both contact pressure and the surface expansion rate, ensuring a superior solid-state bond.

6. Conclusions

In automotive manufacturing, the production of tailored patchwork components is a vital strategy for optimizing the balance between crashworthiness and vehicle weight reduction. However, conventional joining methods can restrict material formability, leading to rupture or cracking during the hot stamping process. To overcome these challenges, this study presents pre-holed hot clinching as a highly efficient, integrated joining solution. To evaluate the effectiveness of this approach, it was compared against forge joining, which, despite its rapid bonding capability within the hot stamping cycle, resulted in insufficient joint strength. These weaknesses necessitated a more robust joining mechanism to meet the load-bearing requirements of ultra-high strength steel assemblies. By utilizing pre-hole geometry, the pre-holed hot clinching process effectively combines a strong mechanical hook with localized solid-state bonding. As a result, the following conclusions were obtained.

(1) Tensile shear strength results demonstrate that joint capacity is highly dependent on pre-hole diameter, peaking at 11.5 kN for the 9 mm pre-hole diameter and significantly surpassing the strength of forge joining, which is limited to an average of 1.2 kN. However, a sharp decline in load-bearing capacity occurs when the pre-hole diameter exceeds 10 mm, as the punch fails to adequately displace material into the oversized cavity, leading to incomplete filling and structural instability.

(2) Cross-tension evaluations further confirm that pre-holed hot clinching is a promising alternative for components subjected to complex, multi-axial loading. Regarding the joining depth, a 60% penetration ratio is established as the optimal threshold for maximizing joint integrity; beyond a 70% ratio, the structural performance deteriorates significantly, defining the upper limit for effective material displacement.

(3) Hardness distribution and microstructural characterization confirm a consistent martensitic transformation throughout the joint region and specimen surface. Coupled with the ausforming effect driven by localized plastic deformation at the clinched portion, this ensures high base strength. To maintain a homogeneous hardness distribution, the gap must not exceed 10 mm to preserve the mechanical properties of the ultra-high-strength steel.

(4) The joint strength is attributed to the dual mechanism of a mechanical geometric anchor and metallurgical solid-state bonding. During deformation, rather than the absolute magnitude of surface expansion rate, it is the relative differential rate between the upper and lower sheets that plays the crucial role in inducing interfacial sliding. This slipping simultaneously drives the formation of the mechanical anchor and segments the brittle Al–Si coating at the pre-hole edge. Unlike forge joining, which relies primarily on weak coating-dominated adhesion with limited substrate interaction, this localized segmentation exposes the underlying steel substrate, achieving a direct, high-strength base-metal bond.

These findings demonstrate that pre-holed hot clinching significantly enhances the mechanical performance of patchwork joints while ensuring integration with the hot

stamping process. Ultimately, this research validates the technique as a superior process for high-performance automotive manufacturing, offering a balance of joint reliability and enhanced processing flexibility.

Author Contributions: Conceptualization, J.C., T.M. and S.S.; methodology, J.C., T.M. and S.S.; software, T.H., J.C. and T.M.; validation, J.C., T.M. and T.H.; formal analysis, J.C., S.S., T.H., T.M. and T.I.; investigation, J.C., T.M. and S.S.; resources, T.M.; data curation, J.C., T.M., T.H. and T.I.; writing—original draft preparation, J.C., T.I. and T.H.; writing—review and editing, J.C., T.M. and S.S.; visualization, J.C., T.I. and T.H.; supervision, S.S. and T.M.; project administration, T.M.; funding acquisition, J.C. and T.M. All authors have read and agreed to the published version of the manuscript.

Funding: This research received no external funding.

Data Availability Statement: The original contributions presented in this study are included in the article. Further inquiries can be directed to the corresponding authors.

Acknowledgments: The authors express their gratitude for the financial support received through the Petchra Pra Jom Klao Ph.D. Research Scholarship from King Mongkut's University of Technology Thonburi.

Conflicts of Interest: The authors declare no conflicts of interest.

References

1. Fan, J.; Meng, X.; Tian, J.; Xing, C.; Wang, C.; Wood, J. A review of transportation carbon emissions research using bibliometric analyses. *J. Traffic Transp. Eng. (Engl. Ed.)* **2023**, *10*, 878–899. [CrossRef]
2. Zhang, W.; Xu, J. Advanced lightweight materials for automobiles: A review. *Mater. Des.* **2022**, *221*, 110994. [CrossRef]
3. Sandrini, G.; Chindamo, D.; Gadola, M.; Candela, A.; Magri, P. Exploring the Impact of Vehicle Lightweighting in Terms of Energy Consumption: Analysis and Simulation on Real Driving Cycle. *Energies* **2024**, *17*, 6398. [CrossRef]
4. Mori, K.; Bariani, P.F.; Behrens, B.A.; Brosius, A.; Bruschi, S.; Maeno, T.; Merklein, M.; Yanagimoto, J. Hot stamping of ultra-high strength steel parts. *CIRP Ann.* **2017**, *66*, 755–777. [CrossRef]
5. Li, J.; Tong, C.; Zhang, R.; Shi, Z.; Lin, J. A data-informed review of scientific and technological developments and future trends in hot stamping. *Int. J. Lightweight Mater. Manuf.* **2024**, *7*, 327–343. [CrossRef]
6. Tisza, M.; Czinege, I. Comparative study of the application of steels and aluminium in lightweight production of automotive parts. *Int. J. Lightweight Mater. Manuf.* **2018**, *1*, 229–238. [CrossRef]
7. Nakagawa, Y.; Mori, K.-i.; Maeno, T. Springback-free mechanism in hot stamping of ultra-high-strength steel parts and deformation behaviour and quenchability for thin sheet. *Int. J. Adv. Manuf. Technol.* **2017**, *95*, 459–467. [CrossRef]
8. Merklein, M.; Johannes, M.; Lechner, M.; Kuppert, A. A review on tailored blanks—Production, applications and evaluation. *J. Mater. Process. Technol.* **2014**, *214*, 151–164. [CrossRef]
9. Krishnamraju, M.; Reddy, P.V.; Appalanaidu, B.; Markendeya, R. Mechanical behavior and forming characteristics of tailor-welded blanks of structural materials: A review. *Multiscale Multidiscip. Model. Exp. Des.* **2024**, *7*, 3133–3151. [CrossRef]
10. Wang, X.; Wang, S.; Lu, R.; Xuan, Y.; Zhang, S.; Zhang, G.; Hu, X.; Liu, X.; Chen, L. Research progresses on technologies and theory of blanks with variable thicknesses. *Materials* **2024**, *17*, 4450. [CrossRef] [PubMed]
11. Gianluca, P.; Gillo, G.; Luca, S. Uniformity of thickness of metal sheets by patchwork blanks: Potential of adhesive bonding. *Frat. Integrità Strutt.* **2020**, *14*, 166–176. [CrossRef]
12. Lei, C.; Xing, Z.; Xu, W.; Hong, Z.; Shan, D. Hot stamping of patchwork blanks: Modelling and experimental investigation. *Int. J. Adv. Manuf. Technol.* **2017**, *92*, 2609–2617. [CrossRef]
13. Shi, D.; Watanabe, K.; Naito, J.; Funada, K.; Yasui, K. Design optimization and application of hot-stamped B pillar with local patchwork blanks. *Thin-Walled Struct.* **2022**, *170*, 108523. [CrossRef]
14. Lara, J.A.C.; Abbade, L.; Mucsi, C.S.; Nizes, A.D.C.; Rossi, J.L. Study of patchwelded blanks resistance spot welding (RSW) before hot stamping with and without heat treatment parameters. *Mater. Res.* **2023**, *26*, e20230053. [CrossRef]
15. Zhang, Z.; Ouyang, X.; Zhu, L. Study on the hot stamping simulation and experiment of A-pillar patchwork blanks. *Int. J. Adv. Manuf. Technol.* **2022**, *122*, 365–376. [CrossRef]
16. Mori, K.-i.; Kaido, T.; Suzuki, Y.; Nakagawa, Y.; Abe, Y. Combined process of hot stamping and mechanical joining for producing ultra-high strength steel patchwork components. *J. Manuf. Process.* **2020**, *59*, 444–455. [CrossRef]
17. Mori, K.-i.; Bay, N.; Fratini, L.; Micari, F.; Tekkaya, A.E. Joining by plastic deformation. *CIRP Ann.* **2013**, *62*, 673–694. [CrossRef]

18. Meschut, G.; Merklein, M.; Brosius, A.; Drummer, D.; Fratini, L.; Füssel, U.; Gude, M.; Homberg, W.; Martins, P.A.F.; Bobbert, M.; et al. Review on mechanical joining by plastic deformation. *J. Adv. Join. Process.* **2022**, *5*, 100113. [CrossRef]
19. Lu, Y.; He, Q.; Chen, Y.; Wang, Y.; Chen, C. A review on the strengthening methods to improve mechanical properties of clinched joints. *Int. J. Adv. Manuf. Technol.* **2025**, *137*, 4435–4469. [CrossRef]
20. Fu, L.; Zhang, S.; Qiu, P.; Xiao, H.; Deng, B.; Lu, X. Optimization of clinching joint process with preforming between ultra-high-strength steel and aluminum alloy sheets. *Metals* **2024**, *14*, 767. [CrossRef]
21. Abe, Y.; Tatara, Y.; Hosokawa, T.; Yamauchi, R. Clinch-bonding process for ultra-high-strength steel and A5052 aluminum alloy sheets. *Materials* **2025**, *18*, 3556. [CrossRef]
22. Lee, C.-J.; Lee, J.-M.; Ryu, H.-Y.; Lee, K.-H.; Kim, B.-M.; Ko, D.-C. Design of hole-clinching process for joining of dissimilar materials—Al6061-T4 alloy with DP780 steel, hot-pressed 22MnB5 steel, and carbon fiber reinforced plastic. *J. Mater. Process. Technol.* **2014**, *214*, 2169–2178. [CrossRef]
23. Chen, L.-W.; Cai, M.-J. Development of a hot stamping clinching tool. *J. Manuf. Process.* **2018**, *34*, 650–658. [CrossRef]
24. Chen, H.; Zhu, Z.; Zhu, Y.; Sun, L.; Guo, Y. Solid-State Welding of Aluminum to Magnesium Alloys: A Review. *Metals* **2023**, *13*, 1410. [CrossRef]
25. Yamagishi, H.; Hisada, Y.; Otsubo, T.; Omori, N. Multilayer bonding of A1N30H foils to A1050 plates using cold spot forge welding. *Heliyon* **2023**, *9*, e23103. [CrossRef] [PubMed]
26. Yamagishi, H. Cu/Al dissimilar cold spot forge welding: Effects of bonding temperature and reduction ratio on joint strength and reaction layer growth. *Metall. Mater. Trans. A* **2023**, *54*, 3519–3536. [CrossRef]
27. Charoensuk, J.; Iwai, T.; Suranuntchai, S.; Maeno, T. Influence of punch shape on joint strength in forge joining of Al-Si-Coated 22MnB5 steel during hot stamping and application to hat bending. *Metals* **2026**, *16*, 376. [CrossRef]
28. *JIS Z 3140*; Method of Inspection and Acceptance Levels for Resistance Spot Welds. Japanese Industrial Standards Committee: Tokyo, Japan, 2017.
29. Japanese Standards Association. *Ferrous Materials & Metallurgy Handbook*; Japanese Industrial Standards Committee: Tokyo, Japan, 2023.
30. Ouyang, X.; Zhang, Z.; Jia, H.; Ren, M.; Sun, Y. Study on the Effect of Heat Treatment on Microstructures and High Temperature Mechanical Properties of Welding Spots of Hot Stamped Ultra-High Strength Steel Patchwork Blanks. *Metals* **2021**, *11*, 1033. [CrossRef]
31. *JIS Z 3136*; Specimen Dimensions and Procedure for Shear Testing Resistance Spot and Embossed Projection Welded Joints. Japanese Industrial Standards Committee: Tokyo, Japan, 1999.
32. *JIS Z 3137*; Specimen Dimensions and Procedure for Cross Tension Testing Resistance Spot and Embossed Projection Weld. Japanese Standards Association: Tokyo, Japan, 1994.
33. Hexagon Manufacturing Intelligence. *Hexagon, Marc 2024.2 Volume A: Theory and User Information*; Hexagon Manufacturing Intelligence: Surrey, UK, 2024.
34. Hexagon Manufacturing Intelligence. *Hexagon, Simufact Forming 2023.3 Application Manual*; Simufact Engineering GmbH: Hamburg, Germany, 2023.
35. Oberpriller, B.; Burkhardt, L.; Griesbach, B. Benchmark 3 Continuous Press Hardening. In *Proceedings of the 7th International Conference and Workshop on Numerical Simulation of 3D Sheet Metal Forming Processes (Numisheet 2008), Interlaken, Switzerland, 1–5 September 2008*; Eidgenössische Technische Hochschule Zürich: Zurich, Switzerland, 2008; pp. 115–129.
36. Xu, Y.; Ji, Q.; Yang, G.; Bao, S.; Zhao, G.; Miao, X.; Mao, X. Effect of Cooling Path on Microstructures and Hardness of Hot-Stamped Steel. *Metals* **2020**, *10*, 1692. [CrossRef]
37. Maeno, T.; Mori, K.-I.; Homma, H.; Talebi-Anaraki, A.; Ikeda, R. Corner Strengthening by Local Thickening and Ausforming Using Planar Compression in Hot Stamping of Ultra-High Strength Steel Parts. *Metals* **2021**, *11*, 1977. [CrossRef]
38. Maeno, T. Hot local compression and die quench ausforming of quenchable steel sheet. In *Proceedings of the Metal Forming 2024*; Materials Research Forum LLC: Kraków, Poland, 2024; pp. 32–40.

Disclaimer/Publisher's Note: The statements, opinions and data contained in all publications are solely those of the individual author(s) and contributor(s) and not of MDPI and/or the editor(s). MDPI and/or the editor(s) disclaim responsibility for any injury to people or property resulting from any ideas, methods, instructions or products referred to in the content.